Politecnico di Torino

Politecnico di Torino

Corso di Laurea Magistrale in Ingegneria Meccanica

A.a. 2021/2022

Sessione di Laurea: Dicembre, 2022

Master's Thesis

Numerical Optimization of High-Pressure Turbine Vanes

Relatori:

Prof. Daniela Anna Misul

Prof. Simone Salvadori

Candidato:

Edoardo Piola

Abstract

Nowadays, the research community of Gas Turbines (GT), driven by the need of maximization of thermal efficiency, attempts to integrate Pressure Gain Combustors (PGCs) to a GT cycle. This technology exploits the isochoric combustions so as to augment the stagnation pressure of the cycle leading to higher efficiency, in contrast to the conventional quasi-isobaric process. One type of PGCs, which gains the community's interest, is the Rotating Detonation Engine (RDE). RDE uses the detonative combustion in order to increase the total pressure. However, harsh outlet conditions with a significant elevated average Mach number are produced for the High-Pressure Turbine (HPT) stage.

The goal of the present thesis is to optimize the CT3 HPT vane for an inlet Mach number equal to 0.6 solving the Reynolds-Averaged Navier-Stokes (RANS) equations. First, the parametrization of the CT3 nominal airfoil is done using B-splines. In the meantime, the endwalls of the hub and the tip are parametrised with the same approach. Furthermore, a variable stagger angle is imposed to the produced airfoil. As a result, a broad Design of Experiments (DOE) of 312 geometries is created varying 18 geometrical parameters of the entire vane. The RANS equation was solved using the commercial solver of ANSYS CFX. Defining appropriately an objective function focusing on the evaluation of the vane's performance, a response surface is created by the results of DOE. In addition, an optimization algorithm predicts the optimal solution for the Stator. In the end, interesting results are uncovered by comparing the baseline configuration with one derived by the optimization process.

Table of Contents:

List of Figures:

List of Tables

Nomenclature:

Symbols:

a, b, c	Parameters for Vertical Parabola;	[/]
A, B, C, D, E, F, G, H, r, q	Parameters in Thickness Equation;	[/]
A', B', c_1, c_2, D'	Parameters in Camber Line Equation;	[/]
c_{ax}	Axial Chord;	[mm]
c_p, c_v	Specific Heat at constant Pressure and Volume;	[J/Kg K]
f, g, h	Objective Functions	[/]
LER	Leading Edge Radius	% of t_{max}
H	Specific Enthalpy	[J/Kg]
k	Specific Heat Ratio;	[/]
M	Mach Number;	[/]
N_{blade}	Number of Blades;	[/]
P	Pressure	[Pa]
P'	Maximum Camber Position	% of c_{ax}
R	Radius;	[mm]

S	Trailing Edge Scale Factor;	% of c_{ax}
T	Temperature;	[K]
TER	Trailing Edge Radius	% of t_{max}
Thick	Thickness	[mm]
t_{max}	Maximum Thickness;	% of c_{ax}
V	Velocity;	[m/s]
X, Y	Absolute Reference Frame;	[mm]
x, y	Rotated Reference Frame;	[mm]
X_T	Maximum Thickness Position;	% of c_{ax}
W_A	Trailing Edge Wedge Angle;	[°]

Greek:

$\alpha, \beta, \gamma, \delta$	Parameters in Camber Line Equation	[/]
β_1, β_2	Leading and Trailing Edge Angles;	[°]
Γ	Degree of Reaction	[/]
$\Delta x, \theta$	Cylindrical Reference Frame	[mm], [rad]
η	Stator Efificiency;	[%]
ξ	Angle Coefficient;	[/]
Θ	Rotation Angle;	[°]
ω	Camber Line Angle	[rad]

Subscripts:

0	Stage Inlet, Input Section;
1	Vane Inlet;
2	Vane Outlet, Rotor Inlet;
3, Out	Rotor Outlet;
E	Vane Exit;
ens	Ensemble;
is	Isentropic;
PS	Pressure Side;
s	Static
SS	Suction Side;
T	Total

Abbreviations:

CCD:	Central Composite Design;
DP:	Design Point;
DOE:	Design of Experiment;
GARS:	Genetic Aggregation Response Surface;
HPT:	High Pressure Turbines;
ICWR:	Internal Combustion Wave Rotor;
J-B:	Joule-Brayton;
LHS:	Latin Hypercube Sampling;
MLS:	Moving Last Squares;
MISQP	Mixed-Integer Sequential Quadratic Programming
MOGA:	Multi-Objective Genetic Algorithm;
NLPQL	Non-Linear Programming by Quadratic Lagrangian
NPR:	Non-Parametric Regression;
PDC:	Pulse Detonation Combustor;
PGC:	Pressure Gain Combustor;
WB:	Workbench;
RDC:	Rotating Detonation Combustor;

RMSE: Root Mean Square Deviation;

RPC: Resonant Pulse Combustor;

RSM: Response Surface Method;

SVM: Support Vector Method;

WB: Workbench;

ZND: Zeldovich-Neumann-Doring;

IGV: Inlet Guided Vane;

Chapter 1

INTRODUCTION

During this Thesis work will be analysed the possibility to allow transonic flows, typical output of a Pressure Gain Combustor (PGC) for High-Pressure Subsonic Turbines.

This topic has been analysed during the past years from several authors, for example, by changing the endwalls shape of the first stage [1], performing a numerical analysis about the efficiency of a Pulsed Detonation Combustor – axial turbine integration with a two dimensions model for both PDCs and Subsonic Turbine [2].

The research will focus on the turbine's stator blade and endwall profile optimization. Indeed an important parameter for the evolution of the flow is in particular the area ratio between throat and inlet that determines the maximum speed of the inlet flow and is defined by the endwall - blade relative position, the total number of blades and their stagger angle.

PRESSURE GAIN COMBUSTOR (PGC)

A Pressure Gain Combustor (PGC), Figure 1, is a power generation developing technology, based on the possibility to obtain an increment of pressure inside the combustion chamber by exploiting shock waves.

It is possible to extract more power with a PGC in respect the classical one, based on the conventional Brayton cycle combustion, because in this second case, the combustion gases leaves the combustion chamber at lower pressure in respect the inlet one (unburned mixture) and this causes a drop in the machine efficiency and work, as the possible expansion ratio in the turbine stage decreases. The combination of heat increase and pressure rise in the PGC offers great potential in terms of thermal efficiency, unlike the unconventional Joule-Brayton cycle [3].

Thanks to this new technologies is possible to obtain a more efficient and cleaner combustion, with a better quality, lower entropy production and consequently a lower fuel consumption. For these reason this research field is also promising in the propulsion area.

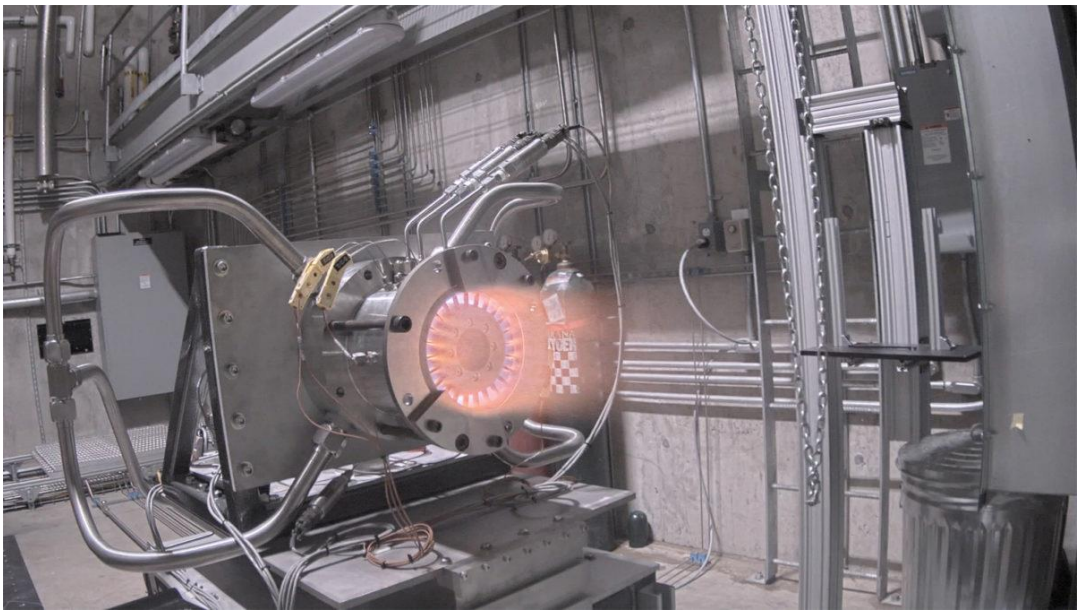

Figure 1: image of the Hydrogen-powered RDC tested at PETAL (Purdue Experimental Turbine Aerothermal Lab) [4].

According to [5] and [6], a study carried out by NASA in 2012 predicts that both intercontinental flight and nitrogen oxide emission should be reduced if such engines can be deployed, while the space exploration field can be improved thanks to these reduced weight and consumption thrusters.

The main Pressure Gain Combustors are:

- PDC: Pulse Detonation Combustor;
- RDC: Rotating Detonation Combustor;
- RPC: Resonant Pulse Combustor;
- ICWR: Internal Combustion Wave Rotor;

PDCs, compared to the classic jet and rocket engines, are working using an intermittent and periodic detonation wave instead of operate through a deflagration of fuel. The flow rate within the combustion chamber is different in the two cases: deflagration ignites the cold fuel by heating it with thanks to the subsonic wave propagation; on the other hand detonation, that has a supersonic flame front, can decompose and activate fuel very quickly through shock waves.
The process in PDCs starts with a deflagrating wave that is first formed in the combustion chamber and next is compressed and heated by the combustion gases through the flame front, producing an increase in the velocity which leads the wave to exceed the sonic threshold and become detonating.
For this kind of flows maximum velocities of the order of M = 5 can be reached, with output flow that belongs either to high subsonic or hypersonic regime.

The pulsating phenomena, where the flow is injected at each cycle between one detonation wave and the next, doesn't have the time to expand inside the combustion chamber, and for this reason could be considered as an evolution with constant volume:

this is an essential point because this kind of combustions are more efficient and therefore require less use of fuel.

For a PDC the thermal energy should be supplied in phase with the acoustic pressure oscillation [6], in order to achieve the maximum efficiency. As a consequence, there's optimum coupling between resonant and operating frequencies and therefore heat is released when the mixture is at maximum compression.

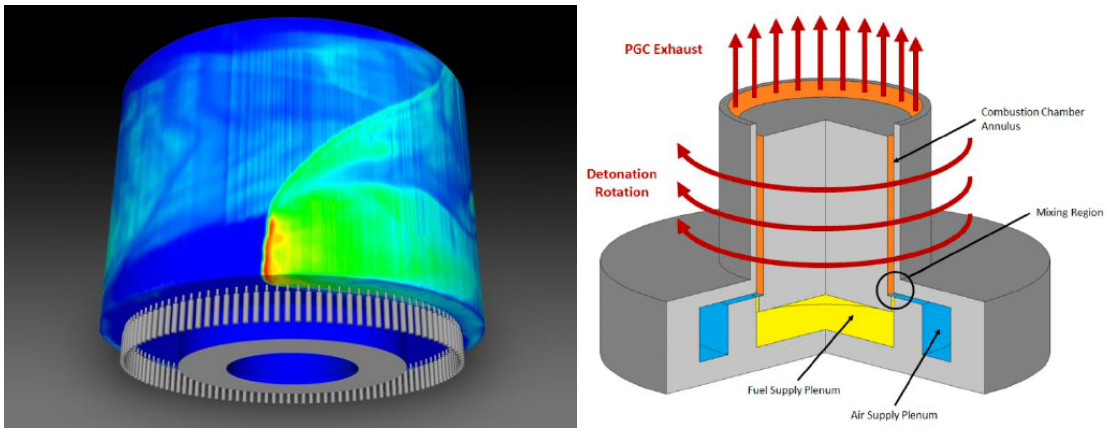

Figure 2: On the left the three-dimensional numerical simulation of a RDE configuration [7]. On the right a sketch of RDE [8].

For what concerns RDE, in Figure 2, the detonation wave moves through a circular annulus so that there will be a supersonic flame front as it uses a detonating wave; igniters are used to activate the fuel-oxide mixture only in the initial phase, because then the detonation reaches enough energy to self-sustain. Once burned, the reaction products exit from the combustion chamber, pushed out from the new incoming mixture.

The exit flow of new PGCs is highly different from the generic outlet flow of a general combustor: it is normally transonic, non-stationary and affected by the fluctuations of pressure, temperature, velocity and flow angle. This point could be a problem for the integration with the downstream turbine that may suffer some issues related to the unstarted condition or efficiency drop.

The aim of this Thesis is the optimization of a single turbine stage that can be efficiently connected to a PGC.

THERMODYNAMIC CYCLES:

In this paragraph will be discussed the useful thermodynamic cycles to describe the thermodynamics of PGCs and their comparison with the conventional Joule-Brayton cycle, whose most standard form in Figure 3 is composed by an isentropic compression (2-3), a constant pressure combustion (3-4), an isentropic expansion (4-5is) and a constant pressure heat transfer (5is-2):

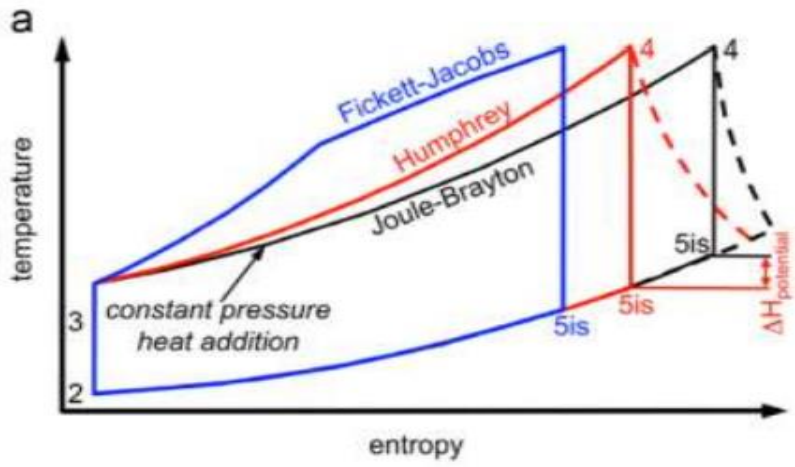

Figure 3: J-B, Humphrey, Fickett-Jacobs cycles comparison on entropic diagram [9].

The described cycle is ideal since, in a real situation, isentropic transformations and a release of combustion gasses at the inlet pressure can't be realized: losses in the various components are present and together with the constant production of entropy lead to a lower efficiency and work than the ideal one.

Figure 3 shows a sketch of the Humphrey cycle that can describe the thermodynamics behind the PGC [9]: the constant-pressure heat addition process of the J-B cycle is replaced with a constant-volume heat addition process. The effect is that the specific volume of gas is kept constant and the pressure increases, leading to an increase of extracted work. The cycle efficiency is related to the maximum temperature T_4 and to the compression ratio.

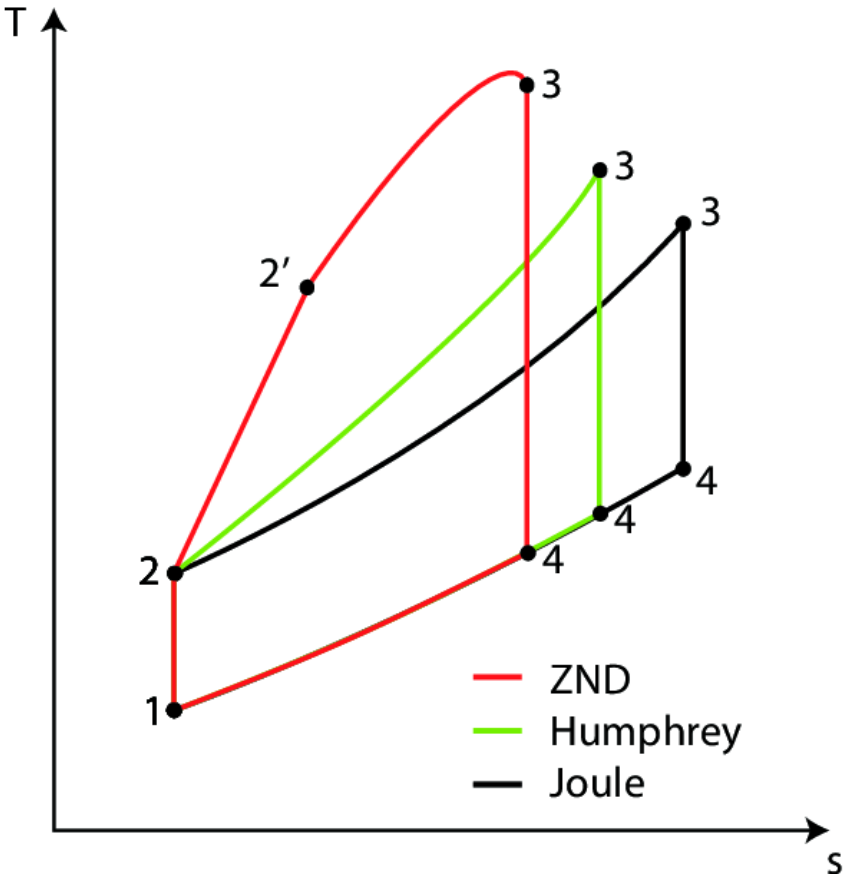

Figure 4: Joule, Humphrey, Zeldovich-Neumann-Doring cycles comparison on entropic diagram [10].

A more realistically combustion process through a detonating wave is represented from the Zeldovich-Neumann-Doring (ZND) cycle in Figure 4, that compared to other cycles, considers a shock wave able to reach a temperature and pressure increase of the combusted mixture.

Referring to Figure 4 it is visible the point 2' of the ZND cycle, called the Neumann point that refers to the encounter of the mixture and the shock wave that causes the relative compression.

The detonative combustion is divided in two consecutive parts: from 2 to 2' the transformation occurs adiabatically through a shock wave that invests the fresh mixture, and from 2' to 3, where occurs a second increase of pressure thanks to the ignition of the mixture, that is burning and moving at the same initial shock wave's speed. The flow is treated as 1-D and stationary and the cycle shows a higher theoretical efficiency in respect with an isochoric combustion [11].

In conclusion, the ZND represents the true physical behavior of the detonating wave only in one 1-D flow hypothesis, and possible problems of excessive temperatures and detonation stability may occur. At the end it is preferred to describe the behavior of PGC with an isochoric combustion, easier to be used and with lower losses and better performances.

RESEARCH OBJECTIVES:

The aim of this research is to present a suitable procedure for the optimization of the first stage of a High Pressure Turbine that shows many problems related to the unstarted turbine. The possible solutions need to satisfy the isentropic limit for subsonic flows, in such a way that the turbine could be self-started, shows Mach Number equal to 0.6 at the entrance value that is more than 3 times higher in respect the nominal one.

This is the reason why it is needed the addition of a diffuser between exit of PGC and Vane inlet, in order to achieve a reduction in the Mass Flow Rate and an optimal Area Ratio in order to reach the design condition for Mach Number.

Many other factors will be taken into account and the diffuser - vane shape will change according to avoid flow separation and to obtain a correct incidence angle on the rotor blade, that will not be analyzed during this activity. This change in the Stator Architecture starts from the definition of CT3 Stator Nominal Configuration, that is analyzed in the next Chapter 2.

Chapter 2

CT3-High Pressure Turbine

Starting from the nominal configuration of CT3 stage, the research will focus on the optimization in terms of efficiency for the Turbine's vane. The CT3 is a High Pressure Turbine Stage made of 43 vanes and 64 rotors (with a pitch to chord ratio equal to 0.7506), values chosen to minimize computational efforts of numerical simulation, minimizing secondary flows [12].

In Figure 5 it is reported the meridional cut of the CT3 stage:

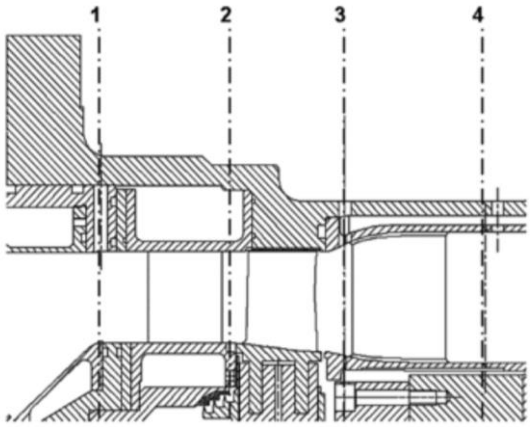

Figure 5: Meridional cut of the CT3 test section [12].

Von Karman Institutes made many studies on this blade various times: one important feature is that can reproduce the operating conditions found in the high-pressure turbine stages of modern engines and gas turbines [13]. For this research only the vane will be considered and the heat transfer between the hot gases and the walls is neglected.

The vane has a 3-D annular geometry that is a cylindrical aerofoil, obtained from the radial stacking of 2-D midsection. Since the rotor blade has a negative lean, the suction side forms an acute angle in respect the hub end-wall that unloads the tip sections reducing tip leakage flows [13].

In the next section will be analysed some useful parameters to evaluate the vane's performance in order to optimize the blade profile in order to ingest a flow with a Mach number around 0.6.

Vane Performance

For the correct simulation of the turbine, some physical parameters are defined in order to set the Boundary Conditions and Output Parameters. In particular it is useful to define the following quantities:

INPUT PARAMETERS

- **Degree of Reaction:** is the ratio of the static pressure drop in the rotating blades of a turbine to the static pressure drop in the turbine stage [14]. According to [15], for our analysis, a convenient value for Γ is 0.314**:**

$$\Gamma = \frac{\Delta H_{s,rotor}}{\Delta H_{T,stage}} = \frac{H_{s2} - H_{s3}}{H_{T1} - H_{T3}} = 1 - \frac{1 - \left(\frac{P_{s2}}{P_{T1}}\right)^{\frac{k-1}{k}}}{1 - \left(\frac{P_{s3}}{P_{T1}}\right)^{\frac{k-1}{k}}} \qquad (1)$$

- **Pressure ratio of the whole stage:** $\frac{P_{T1}}{P_{s3}} = 3.03$, According to [15];

- **Inlet Pressure of the Turbine:** This value is determined from the previous analyses [13] and equal to 161600 Pa;

- Thanks to these three information it is possible to determine the **Outlet Static Pressure from the vane** (P_{s2}) equal to 83289 Pa;

OUTPUT PARAMETERS

- **Efficiency of the Vane:** since the optimization is done only for the vane, the rotor is not considered for the determination of the efficiency. This is not the efficiency of the stage, but it is the one of the vane itself and could be defined thanks to the following:

$$\eta = \frac{V}{V_{is}} \tag{2}$$

Where V is the velocity;

- **The isentropic velocity:**

$$V_{is} = \sqrt{2c_p\left(T_{T1} - T_{Out,is}\right)}; \tag{3}$$

- **The isentropic outlet Temperature**:

$$T_{Out,is} = T_{T1}\left(\frac{P_{s,Out}}{P_{T1}}\right)^{\frac{\boldsymbol{k-1}}{k}} \tag{4}$$

- **Angle Coefficient**:

$$\xi = 1 - \frac{Exit\ Flow\ Angle}{Actual\ Metal\ Angle} \tag{5}$$

CT3 Stator Parameters

As visible in the detail of Figure 5, Figure 6, the Nominal condition of the CT3 Vane has parallel endwalls: The main Nominal Parameters are:

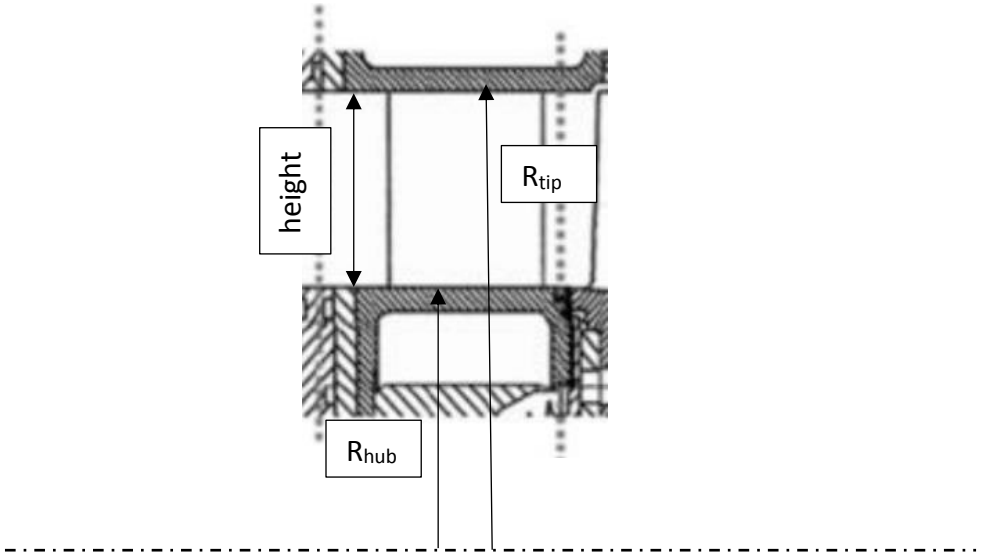

Figure 6: Detail of Figure 5, the Stator Vane with parallel Endwalls from the Meridional Plane Section;

This research will specifically focus on the study of the Stator only then an example of Nominal Vane is reported in the following Figure 7:

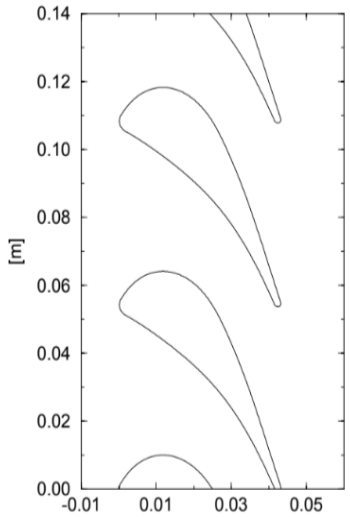

Figure 7: Sketch of the Stator Vane of a CT3 turbine.

Chapter 3

Dunham's Method

J. Dunham provides a parametric method of turbine blade profile design that is requested to satisfy both aerodynamic and mechanical criteria, satisfying the most favourable velocity distribution achievable with the permissible blade thickness [16].

The method is based on the parametrization of the following 8 input physical parameters:

1. Leading edge angle: β_1;
2. Trailing edge angle: β_2;
3. Leading edge radius: LER;
4. Trailing edge radius: TER;
5. Maximum thickness: t_{max};
6. Maximum thickness position: X_T;
7. Trailing edge wedge angle: W_A;
8. Maximum camber position: P;

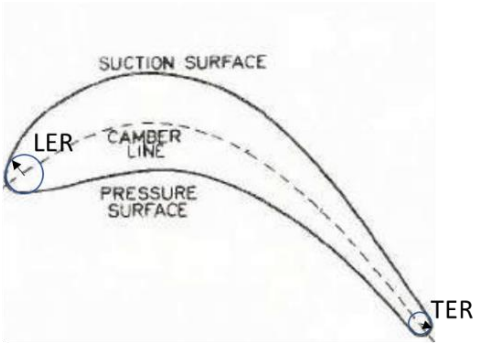

In the following Figure 8 it is shown a sketch of a blade proposed by Dunham with its parameters:

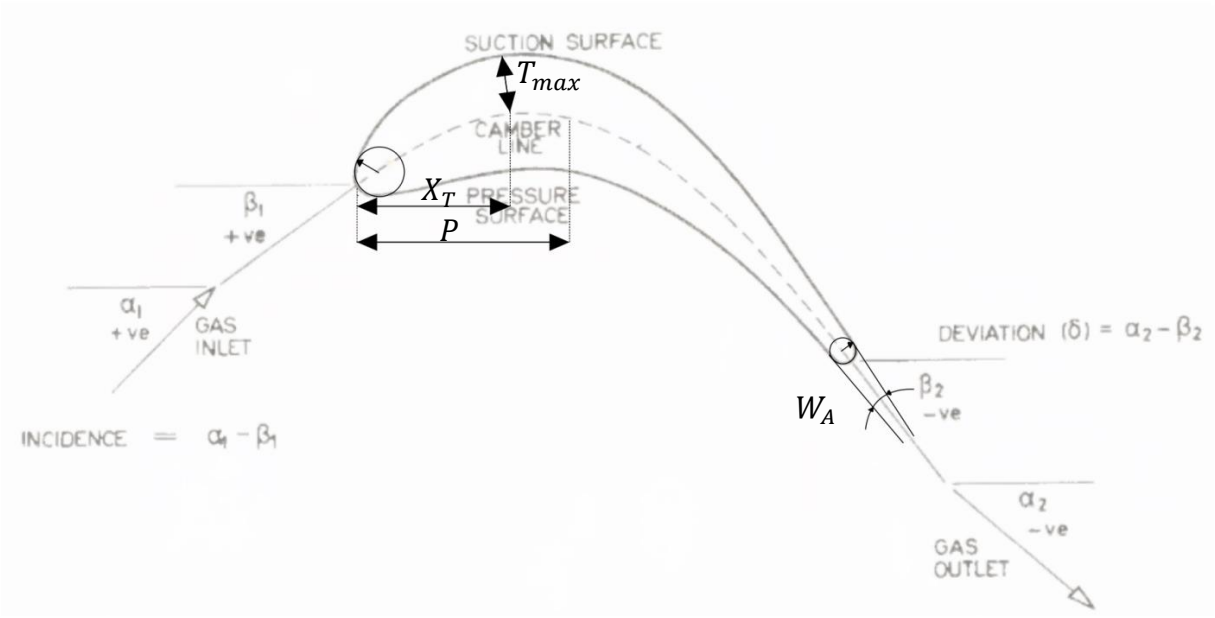

Figure 8: Sketch of a blade proposed by Dunham [16].

For the blade profile generation, Dunham suggests to use a Camber + Thickness approach: after a mean camber line is defined, the value of the thickness is perpendicularly added in both verses, in order to define suction and pressure side of the blade. The opportunity of this method to generate blades inspired to CT3 and LS89 will be analysed in the Chapter 4.

In this paragraph will be described the Camber + Thickness method to obtain blade profiles that are defined by 3 portions:

1. The leading portion from leading edge up to maximum thickness point.
2. The trailing portion from maximum thickness up to the circular trailing edge.
3. The last added circular portion of trailing edge.

The first step of the method consists in the Camber line definition:

CAMBER LINE DEFINITION

A generic Camber line could be defined starting from a rotated parabola. Starting from a simple vertical parabola of equation:

$$Y = aX^2 + bX + c \tag{6}$$

It is possible to rotate the reference frame of an angle Θ:

$$\begin{cases} X = x\cos(\Theta) - y\sin(\Theta) \\ Y = x\sin(\Theta) + y\cos(\Theta) \end{cases} \tag{7}$$

Where (x,y) is the new rotated reference frame.

Substituting Equations (7) in Equation (6) it is possible to obtain the following equation of a generic rotated parabola:

$$\begin{aligned} x\,sin(\Theta) + y\cos(\Theta) = a\left(x\,cos(\Theta) - y\,sin(\Theta)\right)^2 + \\ + b\left(x\,cos(\Theta) - y\,sin(\Theta)\right) + c \end{aligned} \tag{8}$$

It is convenient to write again the Equation (8) by making explicit the y-term:

$$y = \frac{-c_1 - A'x \pm \sqrt{c_2^2 + D'x}}{B'} \tag{9}$$

Where the constants that appears in Equation (9) derive from the recollection of the parameters a, b, c, $sin(\Theta)$, $cos(\Theta)$ in Equation (8); during this mathematical steps is necessary to define the domain of the parameters, that implies the following:

- a>0;
- $\Theta \neq k\pi, with\ k = 0,1,2 \ldots$

The prime derivative of Equation (9) is:

$$y' = \frac{-2A'\sqrt{c_2^2 + D'x} \pm D'}{2B'\sqrt{c_2^2 + D'x}} \tag{10}$$

It is important to notice that the Equation (10) has only 4 independent constants, since B' could be taken into account inside the other constants that appear in the numerator. Applying this simplification, the final relation for the camber line, Equation (11), is obtained:

$$Y_{camber\ line} = \alpha + \beta x \pm \sqrt{\gamma + \delta x} \tag{11}$$

Equation (11) is the final equation of a rotated parabola, and according to Dunham's theory, the camber line ordinate. The first derivative, instead, is:

$$Y'_{camber\ line} = \frac{2\beta\sqrt{\gamma + \delta x} \pm \delta}{2\sqrt{\gamma + \delta x}} \tag{12}$$

To determine the constants of Equation (11) The following boundary conditions are used:

$$\begin{cases} Y(0) = 0 \\ Y(1) = 0 \\ Y'(0) = \tan(\beta_1) \\ Y'(1) = \tan(\beta_2) \end{cases} \tag{13}$$

According to Dunham's definition, if a coordinate system is chosen in which the leading edge is at (0,0) and the trailing edge at (1,0), the slope at the leading edge is $\tan(\beta_1)$ and the slope at the trailing edge is $\tan(\beta_2)$, [16].

The constants of Equation (11) are then:

$$\alpha = \mp\sqrt{\gamma} \tag{14}$$

$$\beta = \pm\sqrt{\gamma} \mp \sqrt{\gamma + \delta} \tag{15}$$

$$\delta = \frac{-4K_2^2 \pm 8K_2\sqrt{\gamma} \pm \sqrt{16K_2^4 + 80K_2^2\gamma \mp 64K_2^3\sqrt{\gamma} \mp 64K_2\gamma\sqrt{\gamma}}}{-2} \quad (16)$$

While γ is defined by the following irrational equation that needs to be solved with an iterating procedure:

$$\mp 2\gamma \mp 2(\sqrt{\gamma(\gamma+\delta)} \pm \delta - 2K_1\sqrt{\gamma} = 0 \quad (17)$$

Since we are only interested in the solutions that belongs to the first quadrant in the Cartesian plane, it's possible to eliminate the unnecessary solutions and obtain the following set of equations:

$$\alpha = -\sqrt{\gamma} \quad (18)$$

$$\beta = \sqrt{\gamma} - \sqrt{\gamma+\delta} \quad (19)$$

$$\delta = \frac{-4K_2^2 + 8K_2\sqrt{\gamma} + \sqrt{16K_2^4 + 80K_2^2\gamma - 64K_2^3\sqrt{\gamma} - 64K_2\gamma\sqrt{\gamma}}}{-2} \quad (20)$$

$$-2\gamma - 2(\sqrt{\gamma(\gamma+\delta)} + \delta - 2K_1\sqrt{\gamma} = 0 \quad (21)$$

To find the value of γ has been chosen to use the Excel solver that implements the non-linear GRG solver to obtain the best approximation of γ that solve the Equation (21).

A mean Camber line is defined substituting Equations (18, 19, 20, 21) in Equation (11). The method proposed by Dunham includes the definition of the thickness distribution.

THICKNESS DISTRIBUTION:

According to Dunham's method [16], the Thickness distribution is defined by the following piecewise function:

$$thick = \begin{cases} 0.1\, t_{max}\left(A\sqrt{x} + Bx + Cx^2 + Dx^3\right), x < 0.01\, XT.S \\ 0.1\, t_{max}\,(E + F(1-x) + G(1-x)^3 + H(1-x)^4, x > 0.01\, XT.S \end{cases} \quad (22)$$

Where S is a scale factor that takes into account the trailing edge radius:

$$S = 1 + TER * T_{max} * 10^{-4} \tag{23}$$

The definition of the thickness starts directly from leading edge up to trailing edge, excluding the final circular part that has to be manually closed at the end of the procedure with a semicircle.

The constants present in Equation (22) are empirically determined as a function of the physical parameters in input: for this purpose Dunham provides the following relations:

$$A = \left(0.08 \frac{LER}{t_{max} S}\right)^{0.5} \tag{24}$$

$$B = \frac{\left(0.3 - \frac{15r}{8} + q\right)}{0.01} XT.S \tag{25}$$

$$C = \frac{\left(-0.3 + \frac{5r}{4} - 2q\right)}{(0.01\, XT.S)^2} \tag{26}$$

$$D = \frac{\left(0.1 - \frac{3r}{8} + q\right)}{(0.01\, XT.S)^3} \tag{27}$$

$$E = 0.002\, TER \tag{28}$$

$$F = \frac{20 \tan\left(\frac{W_A}{2}\right)}{t_{max} S} \tag{29}$$

$$G = \left[0.4 - 0.008\, TER - \frac{60 \tan\left(\frac{W_A}{2}\right)}{t_{max} S}(1 - 0.01\, XT.S)\right](1 - 0.01\, XT.S)^{-3} \tag{30}$$

$$H = -\left[0.3 - 0.006\,TER - \frac{40\tan\left(\frac{W_A}{2}\right)}{t_{max}S}(1 - 0.01\,XT.S)\right](1 - 0.01\,XT.S)^{-4} \quad (31)$$

$$r = \left(0.0008\,LER.\frac{XT}{t_{max}}\right)^{0.5} \quad (32)$$

$$q = \left[-0.6 - 0.012\,TER - \frac{60\tan\left(\frac{W_A}{2}\right)}{t_{max}S}(1 - 0.01\,XT.S)\right]\left(\frac{0.01\,XT.S}{1 - 0.01\,XT.S}\right)^2 \quad (33)$$

Once Camber and thickness are defined, according to the theory, it's possible to obtain the blade profile.

BLADE PROFILE GENERATION

The blade profile is made up of two symmetric sides in respect the camber line: the portion below the Camber is called Pressure side, while the upper one is the Suction side.

The profile is generated from the addition of the thickness perpendicularly to the camber line for every point in the following way:

$$x_{ss} = X_{camber\ line} + \frac{thick}{2}\cos\omega \qquad y_{ss} = Y_{camber\ line} + \frac{thick}{2}\sin\omega \quad (34)$$

$$x_{ps} = X_{camber\ line} - \frac{thick}{2}\cos\omega \qquad y_{ps} = Y_{camber\ line} - \frac{thick}{2}\sin\omega \quad (35)$$

Where ω is the slope of the camber line for every point:

$$\omega_i = \text{atan}\left(\frac{Y_{camber\ line,i+1} - Y_{camber\ line,i}}{X_{camber\ line,i+1} - X_{camber\ line,i}}\right) \qquad (36)$$

To understand better the concept of adding thickness to camber line, the following sketch is depicted in Figure 9:

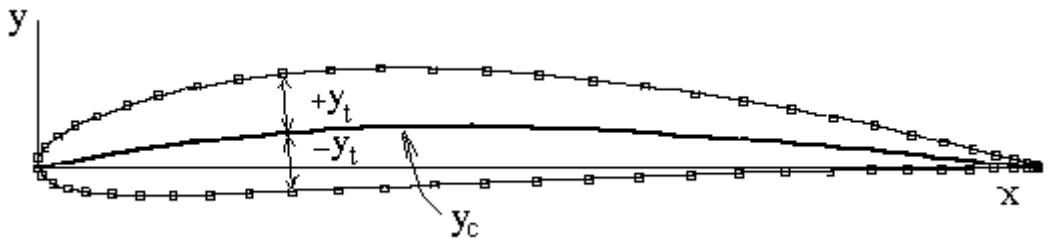

Figure 9: Computer Program to Obtain Ordinates for NACA Aerofoils [17].

Chapter 4

Dunham's Method Results:

In this chapter will be shown the results obtained by following Dunham's procedure described in Chapter 3.

The method is implemented in ANSYS Workbench and has the following architecture, showed in Figure 10:

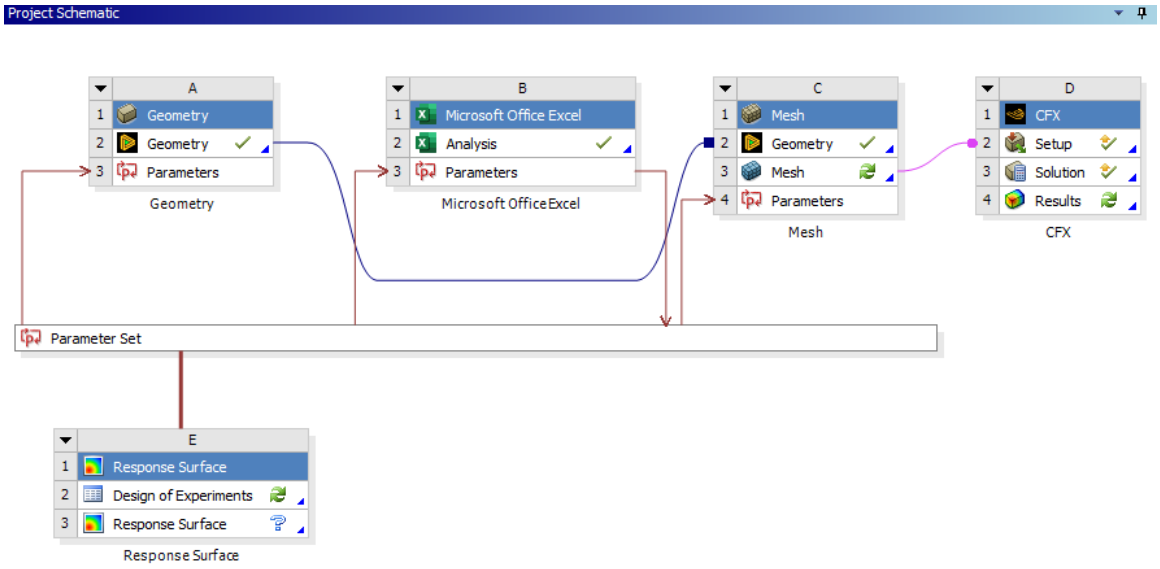

Figure 10: Workbench Project Scheme.

The model starts with the generation of the 3D geometry of the blade, thanks to the DesignModeler tool BladeEditor that is able to build blade profiles from the Camber + Thickness method.

BLADE PROFILE DEFINITION

The profile definition starts from the control volume specification: the tool used to build the blade (BladeEditor) requires a domain with upper and lower bound, respectively hub and shroud in Figure 11 parallel to the machine axis:

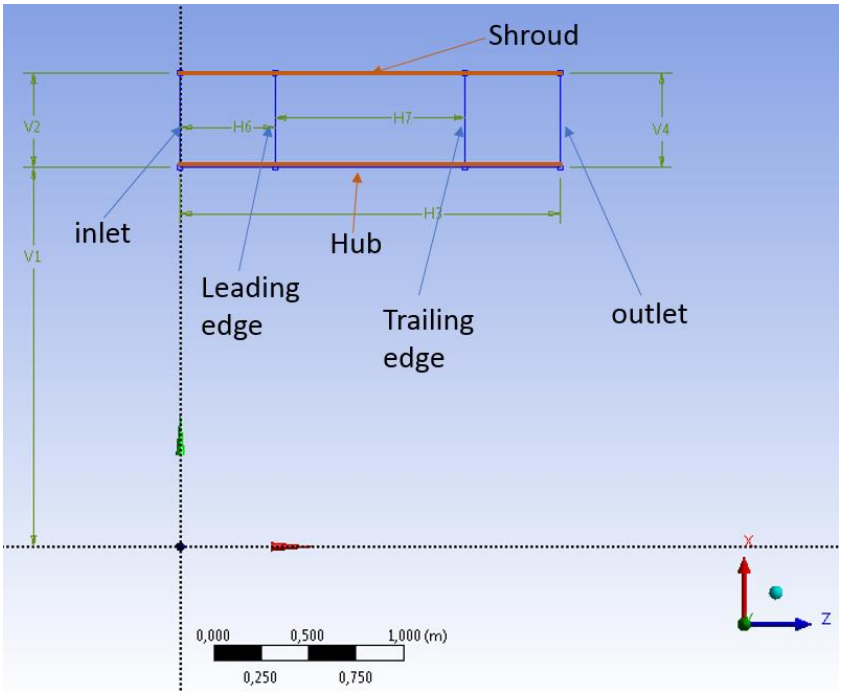

Figure 11: BladeEditor FlowPath: control volume for the generation of the vane.

The blade will lie in-between the Leading and Trailing edge, and the chord length is defined by the distance of these two segments. Every parameter will be normalized in respect of the chord.

The tool BladeEditor can generate blade profiles starting from the Camber + Thickness definition: in this Thesis it is followed this procedure:

1. Define a Camber line for the layer at the hub as a Spline passing through 16 points controlled as parameters;
2. Define a Thickness distribution for the layer at the hub as a Spline passing through 11 equally-spaced points controlled as parameters;
3. Repeat points 1 and 2 for the layer at the shroud.

The points on the camber line in Figure 12 are not equally spaced, but the leading edge portion shows a concentration of point, in order to interpolate in the best way possible the Camber line in the first part, where the inlet angle has to be the most precise as possible, to avoid incidence problems.

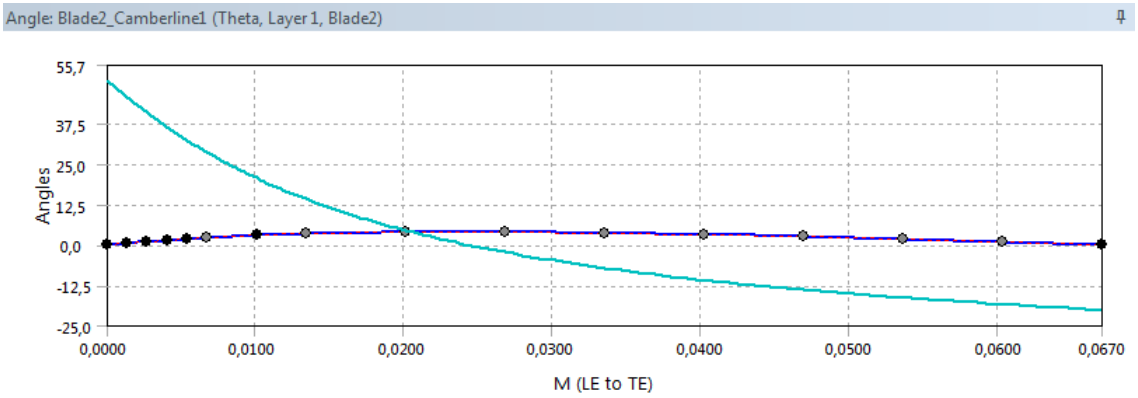

Figure 12: Camber Line definition on DesignModeler's BladeEditor.

The points are controlled as parameters thanks to the workbench tool "parameter set" and the law that controls their position is defined in Chapter 3 from the Equation (11) and the Equation (22).

The irrational Equation (21) that finds the value of γ is solved with the use of Microsoft Office Excel tab in Figure 10 where the Excel automatic solver is used. To automatize the code, a Macro function in Excel has been created, in order to run many simulations consecutively without interruptions. For this reason it's fundamental to activate the Macro box in the properties of workbench project.

It is important to underline that BladeEditor works with cylindrical coordinates and the ordinate of the camber line in Figure 12 is an angle: for this reason it is necessary to apply the following change in the coordinates (Figure 13) where Y_{camber} becomes θ.

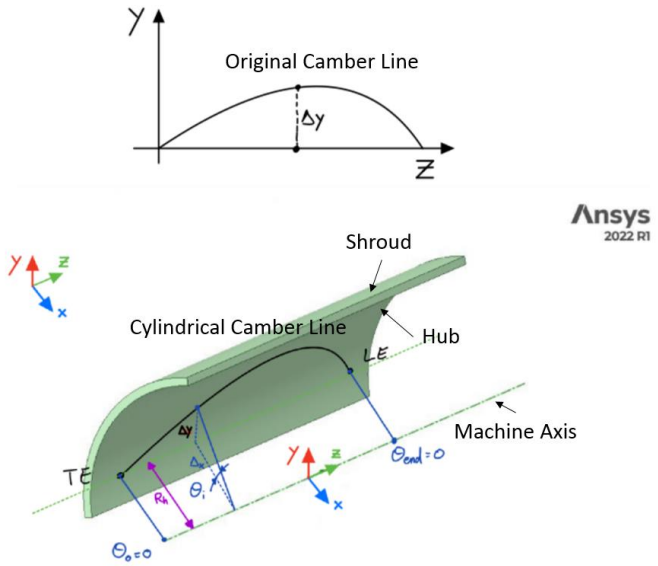

Figure 13: Original (Cartesian) Camber line on plane Z-Y – Camber line projected on a cylindrical surface.

$$\theta = \operatorname{atan}\left(\frac{\Delta y}{\Delta x}\right) \tag{37}$$

$$\Delta y = Y_{camber} \tag{38}$$

$$\Delta x = Radius \rightarrow R_{hub} or\ R_{shroud} \tag{39}$$

$$\theta_{hub} = \operatorname{atan}\left(\frac{Y_{camber}}{R_{hub}}\right) \tag{40}$$

$$\theta_{shroud} = \operatorname{atan}\left(\frac{Y_{camber}}{R_{shroud}}\right) \tag{41}$$

The values obtained for θ at the hub and shroud, Equations (40) and (41), are related to the Equations described in Chapter 3 and every control point in Figure 12 is controlled as parameter starting from a x-coordinate (axial chord) and evaluating the corresponding θ_{hub} and θ_{shroud}, that depend on the value of the radius.

The following Figure 14 it is represented to better understand the scheme of the parameter tab used to control the points in Figure 12;

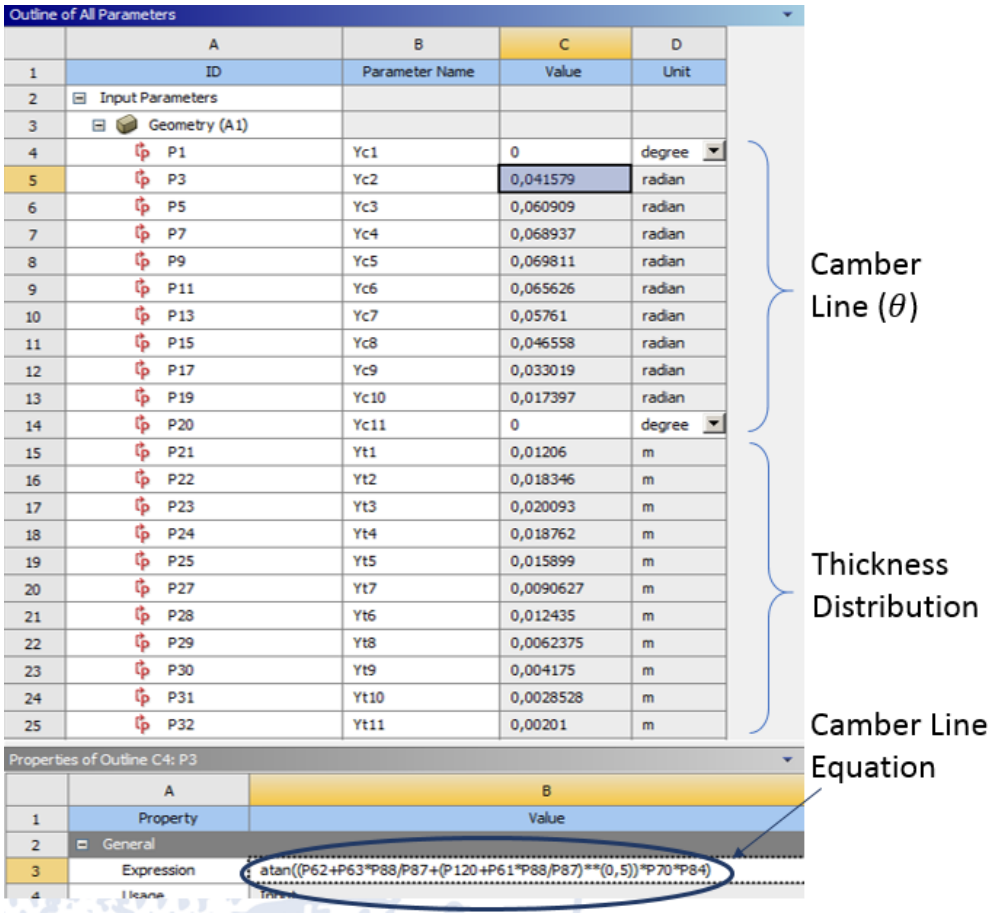

Figure 14: Outline of some Input Parameters on Workbench.

The terms present in the example of Camber line equation are the terms of the Equation (11) in Chapter 3, while the term P88/P87 is the normalized abscissa in respect of the chord.

For what concerns the thickness distribution, the reference frame is Cartesian and not cylindrical: there's still a difference with Dunham's method, because the first control point is not starting with zero thickness, since for the CAD it's impossible to generate such a geometry.

As mentioned in Chapter 3, Dunham's thickness distribution starts from the leading edge with an initial value of zero, while the Workbench's one starts with a value equal to the leading edge radius, as it is shown in Figure 15. The trailing edge thickness instead equals Dunham's , since for that portion, the definition of the two methods is the same. The equation used to control the Spline points is described in Chapter 3.

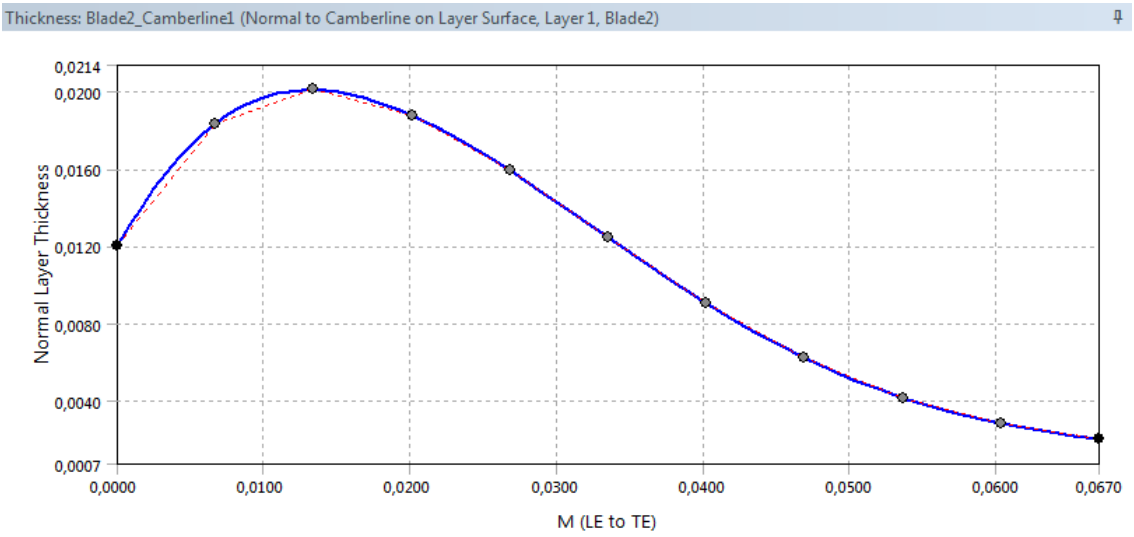

Figure 15: Thickness distribution definition on DesignModeler's BladeEditor.

Once both Camber line and thickness are defined, the tool can generate the 3D blade profile: only one blade is created and its chord is axial and therefore with zero stagger.

STAGGER ROTATION AND SIMULATION CONTROL VOLUME:

First the blade profile is generated, later it is rotated on the YZ plane in order to reach zero incidence, in order to have a direction of the inlet flow that is horizontal. The rotation angle is equal to the inlet angle of the blade β_1.

It's necessary to find a sensible control volume in order to run the simulation as accurate as possible and with less number of iterations. For this aim a periodic control volume is chosen by isolating the blade in-between an upper and a lower line (periodic boundaries in green in Figure 16. The distance between the two lines is equal to the pitch, and depends on the distance with machine axis (machine radius) and the number of blades present.

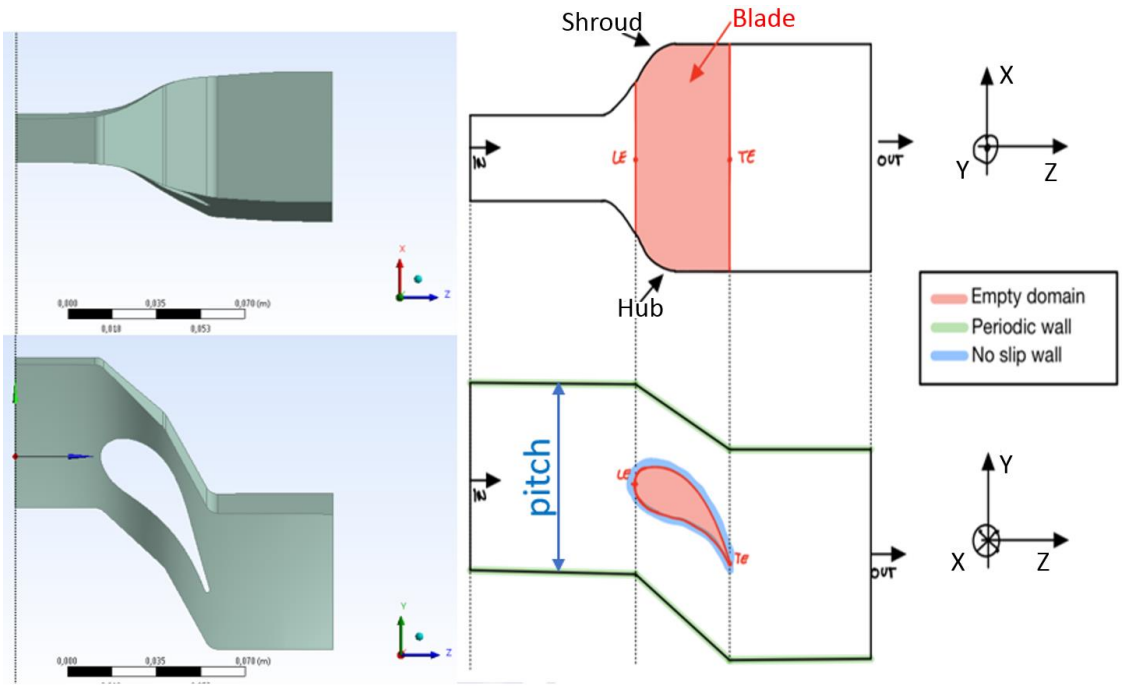

Figure 16: Sketch of the Endwalls and Blade Profile on X-Z and Y-Z planes.

On plane XZ it is visible the endwall contour that is made of a Spline curve controlled by 8 points per side. This shape of the diffuser is necessary in order to obtain the desired boundary conditions, for example a Mach number equal to 0.6 at the inlet; in the following Table 1 are shown the coordinates of the Spline control points in Figure 8, taken from the past studies [13].

Table 1: Initial position of Endwall control points.

	Z [m]	X [m]
Point 1	0	0.35625
Point 2	0.02	0.35625
Point 3	0.0415	0.35625
Point 4	0.05734	0.34435
Point 5	0.07308	0.34135
Point 6	0.106242	0.3395
Point 7	0.107242	0.3395
Point 8	0.125242	0.3395
Point 9	0	0.37345
Point 10	0.02	0.37345
Point 11	0.0415	0.37345
Point 12	0.05734	0.38535
Point 13	0.07308	0.38835
Point 14	0.106242	0.3902
Point 15	0.107242	0.3902
Point 16	0.125242	0.3902

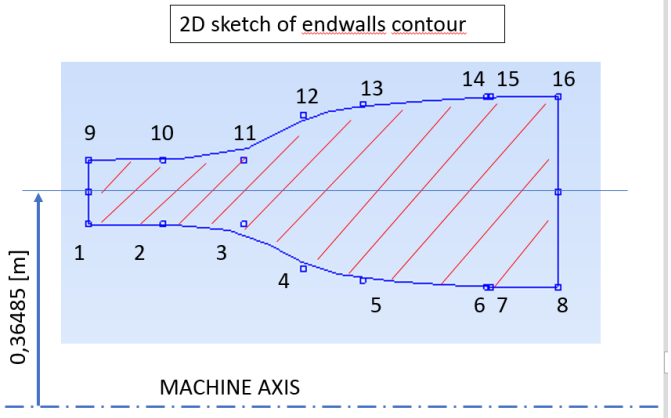

Figure 8: Sketch of the Endwall's profile B-splines.

In the following Figure 9 is showed an example of total complexive domain with 24 blades and its reduced domain with periodic boundaries: the walls of the blade are imposed as non-slip walls and the flow is set by a difference in pressure between inlet and outlet.

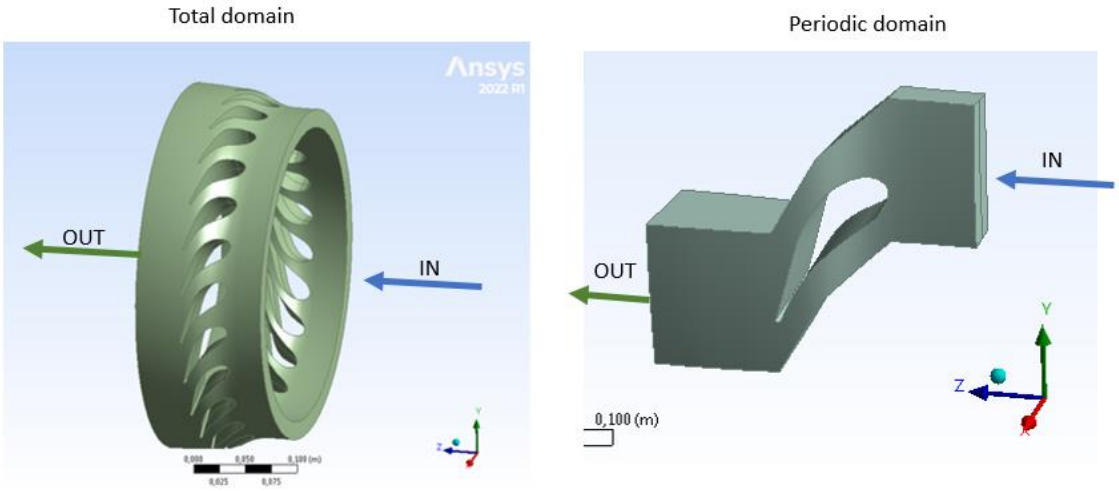

Figure 9: Total and Periodic Control Volume of the Turbine Vane.

HPT EXISTING BLADES PARAMETERS EXTRACTION:

Since the objective of this Thesis is to reproduce and optimize an existing high pressure turbine blade, for example the one discussed in Chapter 2, it is necessary to make a comparison between the blades generated with DesignModeler thanks to Dunham's method and the CT3 and LS89 HPTs.

In order to generate similar profiles to the existing HPTs it is necessary to extract the physical parameters from CT3 and LS89. Thanks to this approach it's possible to set those parameters as input for the workbench code and try to obtain comparable results.

In literature are available some of the physical parameters [18], others instead has to be determined with a MatLab code: thanks to the points on suction and pressure side of the two existing blades it is possible to analyse the profile on MatLab and apply some mathematical considerations in order to extract the physical parameters. For example it is possible to extract the mean camber line from a given profile following this algorithm:

1. Starting from a point on the pressure side, some circles increasing the radius every step are built;
2. For every circle, the distance between the centre and the corresponding point on the suction side is compared with the actual radius of the circle, leading to an error;

3. For every point on the pressure side will be found a point of the camber line, in order to minimize this error;

In the following Figure 10 it is represented an example of circles, whose centres are points of the Camber line; only a few circles are represented in order to be clear and don't overload the image.

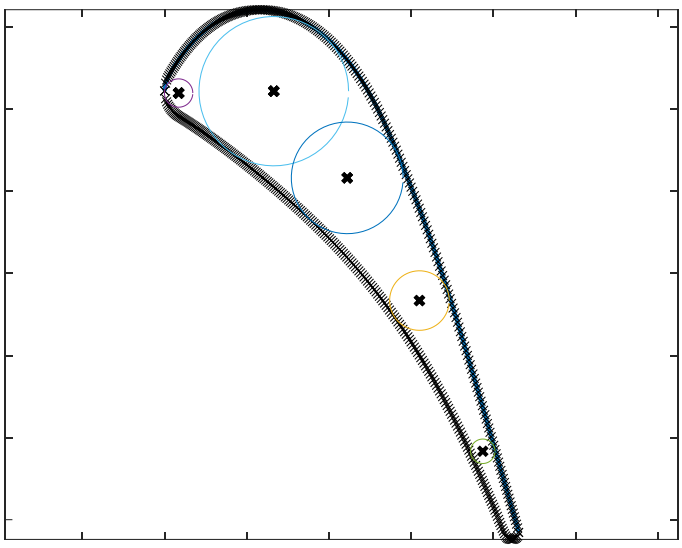

Figure 10: MatLab representation of Camber line evaluation: the 5 centers of the circles in figure are only some of the point used to determine Camber line.

This procedure is performed starting from all the points on the pressure side, obtaining the following result in Figure 20:

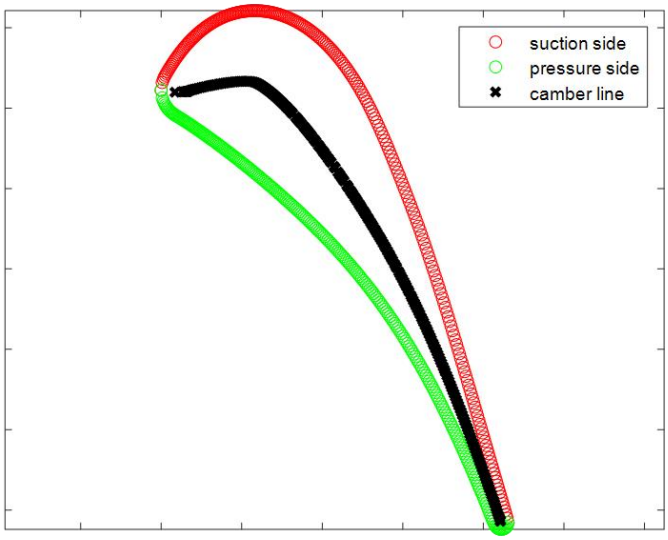

Figure 20: The Camber line obtained thanks to the MatLab script.

From the mean Camber line is possible to find the value of outlet angle β_2, since corresponds to the line's slope at the trailing edge, and the maximum thickness with its position.

To find the maximum thickness and its position, the perpendicular distance in respect the Camber line up to suction side is found on MatLab as shown in Figure 21, and the maximum one is chosen as T_{max}.

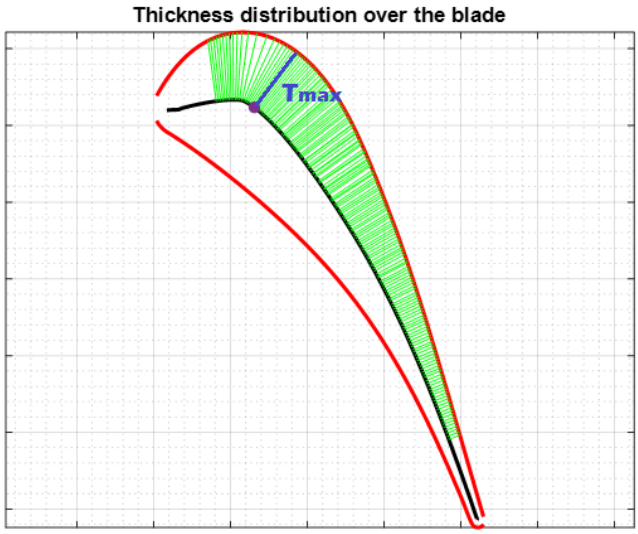

Figure 21: Thickness distribution over the vane and Maximum Thickness position.

BLADE COMPARISON WITH HPT:

In order to make a comparison between the existing blades and the WB-generated ones, the profile points of the CT3 and LS89 blades are extracted from literature [18] and compared on MatLab with the points of the WB generated blades extracted from the mesh nodes.

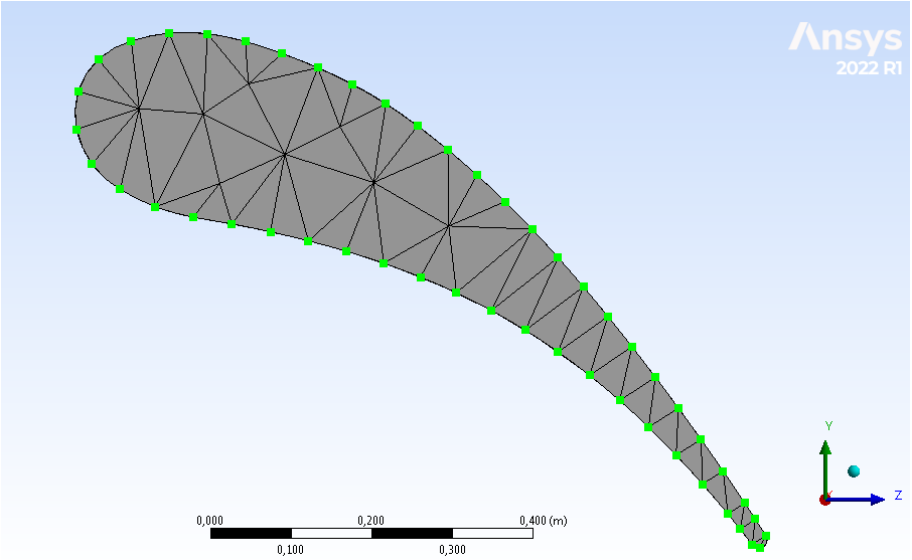

Figure 22: Pressure and Suction Sides points extraction.

In Figure 22 are displayed in green the nodes extracted from a blade profile on workbench.

With the physical parameters of the existing blades found in the previous paragraph, a blade profile is realised. This set of input parameters has a leading edge radius too small to give feasible solutions and the maximum thickness position X_T is too near to the leading edge point, showing as result a change in the curvature on the pressure side (Figure 11 a).

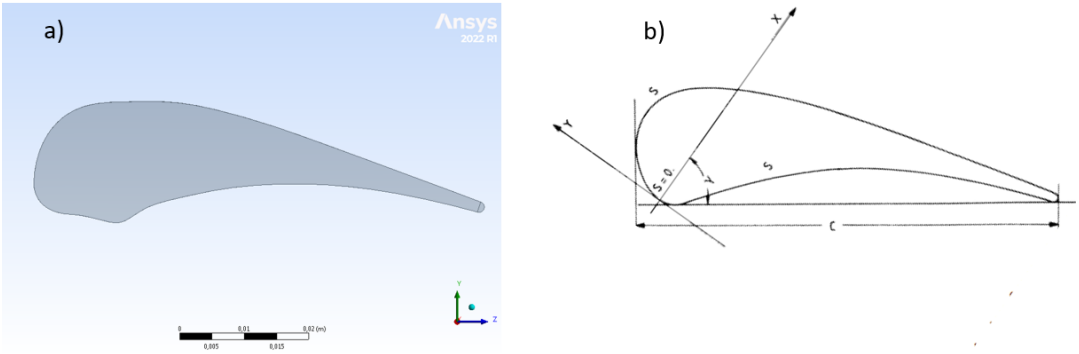

Figure 11: Comparison between the nominal LS89 profile (Figure b) [18] and the profile obtained with the same input physical parameters using the mentioned Method (Figure a).

To overcome this problem some trials with higher values of LER and X_T are done (Figure 12): The lowest acceptable value for LER was 50 for LS89 (in respect of 23) and 55 for the CT3 (in respect 20), while for X_T the lowest value for LS89 is 16.5 (in respect 8) and for CT3 is 12 in (in respect 8.5).

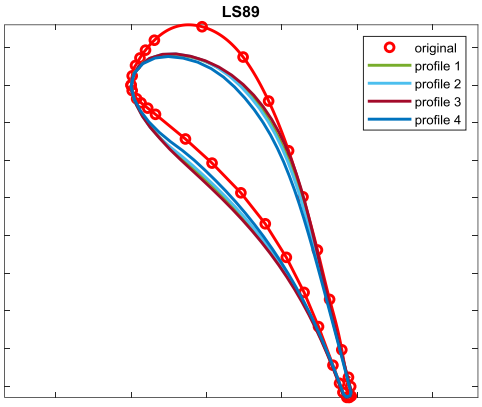

Table 2: Input trials Physical Parameters to reproduce LS89 Vane

	LS89	Profile 1	Profile 2	Profile 3	Profile 4
LER	23	50	50	55	55
TER	4.5	4.5	4.5	4.5	4.5
tmax	27	27	25	24.5	26
XT	8	18	18	16.5	20
Wa	6.5	6.5	6.5	6.5	6.5
beta1	55	55	55	55	55
beta2	-18	-18	-18	-18	-18

Legend:
- Exact value
- Changing values

Figure 12: 4 trial profiles with similar physical parameters in respect LS 89 Vane.

The value of T_{MAX} is important, since the radii values are linked to it and the workbench profile (as visible in Figure 25) shows a pressure and suction sides below the original one: If the value of T_{MAX} is increased, the suction side may better follow the original one, but the pressure side is going to be farthest.

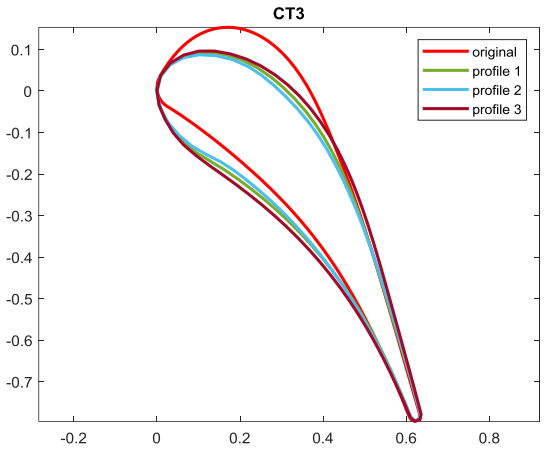

Table 3: Input trials Physical Parameters to reproduce CT3 Vane

	CT3	Profile 1	Profile 2	Profile 3
LER	20	60	55	60
TER	5	5	5	5
tmax	26.6	25	23	26.6
XT	8.5	15	12	18
Wa	6.5	6.5	9	9
beta1	51	51	51	51
beta2	-20	-20	-20	-20

Legend:
- Exact value
- Changing values

Figure 25: 3 trial profiles with similar physical parameters in respect CT3 Vane.

CONCLUSIONS

In this paragraph the Dunham's method has been analysed and its application to the design and parametrization of a High Pressure Turbine blade. The limits of Dunham's approach are specially related to the leading edge radius and the maximum thickness

position, parameters that for the type of blades that are intended to be reproduced, are crucial. In particular it's important to highlight how the maximum thickness horizontal position X_T is out of the valid range in order to reproduce an aerodynamic profile, since the resulting geometry presents a big change in curvature.

The conventional HPTs analysed in Chapter 2 are not reproduced with Dunham's method. For this reason the previous approach [13] of generating a blade profile by controlling B-spline points is used. In the next Chapter 5 a brief explanation of this method is described.

Chapter 5

B-spline Method for Stator Optimization

The method analysed during the previous chapter might be suitable for low-pressure turbines, but in our study, where only high pressure turbines are considered, the target is defined by the existing blades CT3 and LS89 and for this reason Dunham's method is not suitable.

During previous studies performed by N. Rosafio and F. Civerra [13] a method for the CAD implementation of a high pressure turbine blade profile is analysed. The procedure consists in the parametrization of a blade profile (and its endwalls) thanks to the definition of many control points of a B-spline curve: The total number of points is 7 for the Suction Side and 5 on the Pressure Side; the leading and trailing edges are closed thanks to a semicircle.

Method Definition: Geometry generation

The method tries to reproduce the CT3 High Pressure Turbine Blade profile thanks to the definition of two B-spline curves:

1. The Suction Side is defined by 7 points;
2. The Pressure Side is defined by 5 points;

The starting points are obtained in order to reproduce the nominal CT3 blade, as it is represented in the following Figure 26:

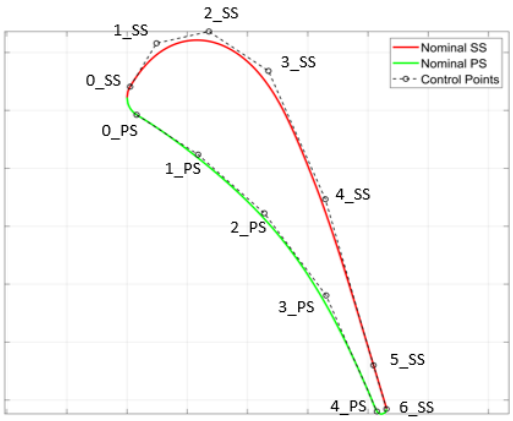

Figure 26: Scheme for the Controlled point used to reproduce the CT3 vane's shape.

During the previous researches, a sensitivity analysis on the control points was done: for this reason it is possible to select only some points to be controlled during the generation of the Design of Experiment samples Table 4; in particular the points that are changed are:

Table 4: Upper and Lower bounds for the position of Controlled Vane's points.

Point ID:	Reference Frame	Min Value X [mm]	Max Value X [mm]	Min Value Y [mm]	Max Value Y [mm]
Point 0 (SS)	Relative to Point (-10,0)	2	11	2.7	4.5
Point 1 (SS)	Relative to Point 0 (SS)	2	7	Fixed	
Point 2 (SS)	Absolute	11	15	8.6	17
Point 3 (SS)	Absolute	21	26	5	10
Point 4 (SS)	Absolute	32	33.2	15	16
Point 5 (SS)	Fixed				
Point 6 (SS)	Fixed				
Point 0 (PS)	Absolute	Fixed		0.6	0.9
Point 1 (PS)	Absolute	Fixed		7	8
Point 2 (PS)	Absolute	20	25	15.5	18
Point 3 (PS)	Fixed				
Point 4 (PS)	Fixed				

The total number of controlled vane's parameters is equal to 13. In Table 4 are represented the controlled points of the vane and their range of values, that is found thanks to an iterative procedure, where the starting upper and lower bounds are randomly guessed and chosen in respect the number of valid profiles generated within this range.

In order to determine a correct and real behaviour of the stage, also the endwalls are changed during the research: thanks to this approach it is possible to study the different results and effects on the flow and inlet Mach number.

In Figure 27 it is reported the sketch of the upper symmetric side of the endwalls, that is determined by a B-spline curve defined from 6 control points:

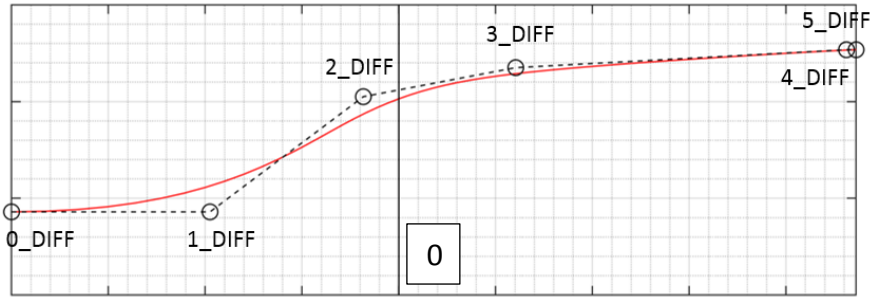

Figure 27: Scheme for the Controlled point used to reproduce the Endwall's shape.

As done for the vane in Table 4, the Table 5 reports the upper and lower range for the Endwall's controlled points:

Table 5: Upper and Lower bounds for the position of Endwall's points.

Point ID:	Reference Frame	Min Value X [mm]	Max Value X [mm]	Min Value Y [mm]	Max Value Y [mm]
Point 0 (ENDWALL)	Absolute	Fixed			
Point 1 (ENDWALL)	Relative to point 0 (SS)	36.5	44.5	Fixed	
Point 2 (ENDWALL)	Relative to Point 1 (ENDWALL)	19.4	23.6	Fixed	
Point 3 (ENDWALL)	Relative to Point 2 (ENDWALL)	14.3	17.2	Fixed	
Point 4 (ENDWALL)	Relative to Point 3 (ENDWALL)	14.2	17.2	Fixed	
Point 5 (ENDWALL)	Absolute	Fixed			

Point 1 of the endwall is defined in respect the first point on the suction side that is a moving reference frame. For this reason it is not possible to define a priori the shapes and positions of the endwall points.

As last step, the Blade is tilted in respect the leading edge according to a small stagger angle that is changed from 0 to -5°.

Finally, it is possible to visualize the domain in which all the profiles are generated: In the following Figure 13 are shown in different grey scales all the possible vane profiles that can be realized from the analysis of Design of Experiment, in respect the red dashed line that represents the nominal profile:

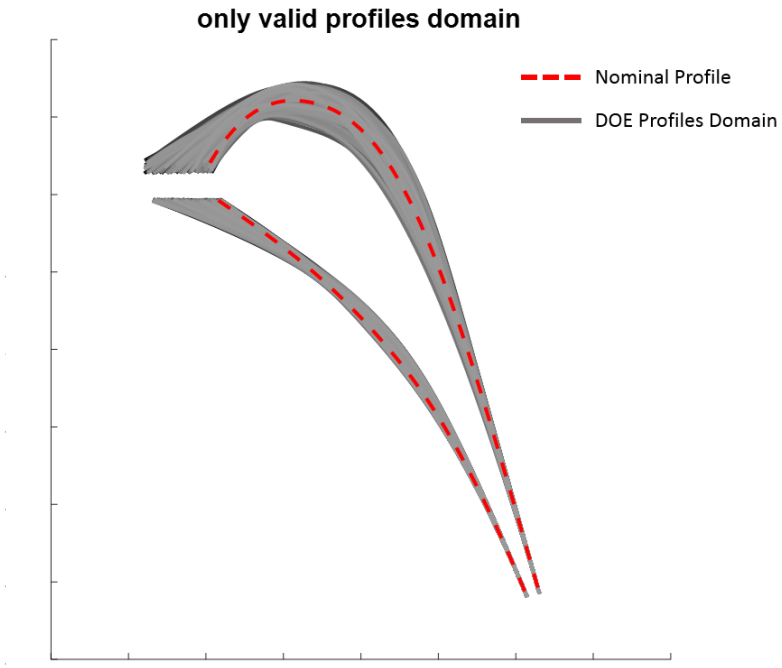

Figure 13: Region in which the Vane Profiles can be generated.

Since the endwalls are generated starting from the position of the first vane point on suction side, the domain of endwalls + vane + stagger is generated in the following way:

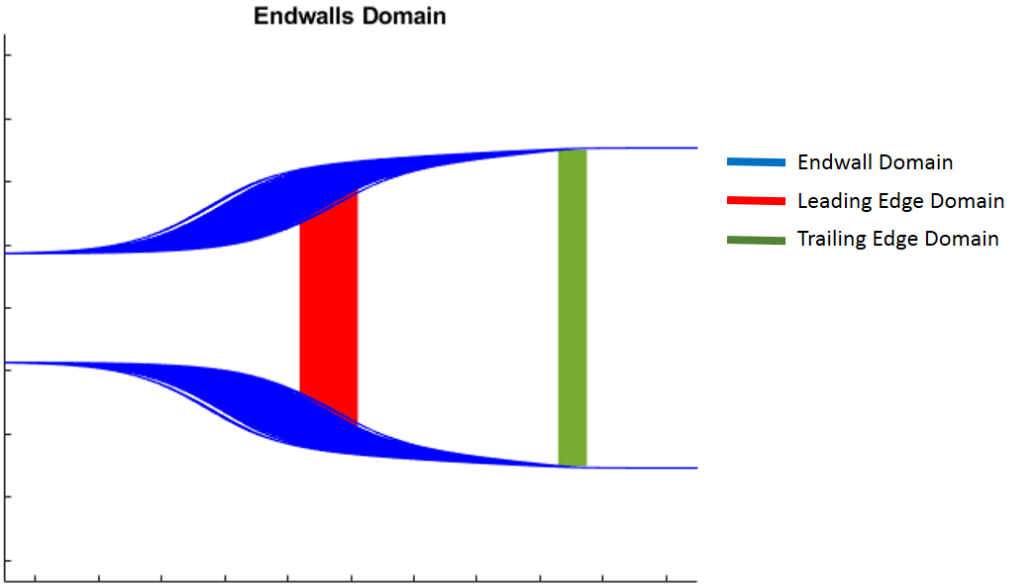

Figure 14: Region in which the Endwalls Profiles can be generated.

The Leading Edge (in Figure 14 in red) changes its position according to Figure 13 and the first controlled point of the endwalls changes its relative position in respect of this first point. In blue it is shown the domain in which all the possible endwalls configuration can be generated, while the green vertical lines are representing the trailing edge that is changing its position according to the stagger angle.

The 3-D control volume is defined from the revolution of the endwall domain without the blade profile: the revolution axis corresponds to the machine one (-369.85 mm from midspan, parallel to the absolute X-axis) and the extrusion is done for $\frac{360}{N_{blades}}$ degrees, in order to simulate the periodicity of the stage for a different number of blades. In Figure 30 it is reported an example of 3D control volume:

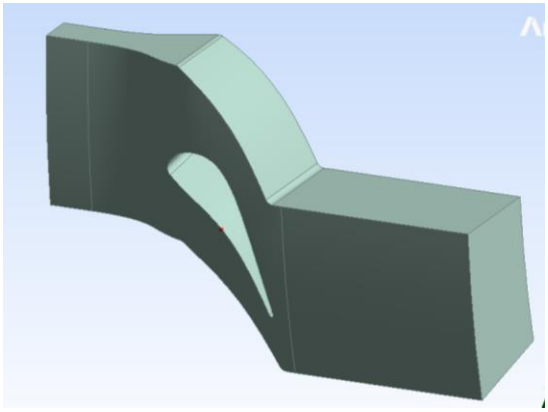

Figure 30: Example of 3-D Periodic Control Volume.

The two perpendicular upper and lower surfaces normal to the Y-axis are defined by pressure side elongated with two horizontal portions, one before the leading edge and one after the trailing edge. The distance between upper and lower surface is determined from the pitch between two blades.

Method definition: Mesh generation

Once the geometry is defined, a frozen cube is added to the DesignModeler project in the following way, as represented in Figure 31:

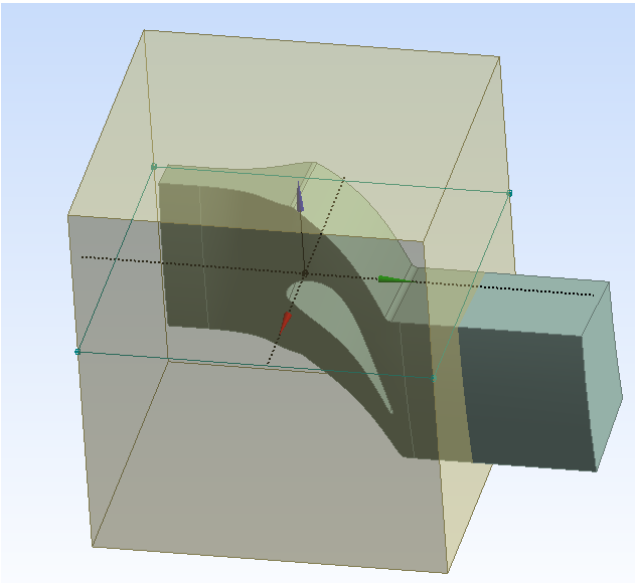

Figure 31: Frozen Cube addition for the Mesh refinement.

The cube is an auxiliary geometry used to refine the mesh in the first portion of domain, up to one nominal axial chord after the trailing edge.

The mesh is performed starting from the following properties:

- The last part of control volume has a mesh size of 5mm (out of the auxiliary cube);
- The control volume contained in the auxiliary cube has a finer mesh size (1.5 mm) and 20 inflation layers 1mm thick;
- The total number of elements is in the order of magnitude of 2e6;

In Figure 15 it is reported an example of mesh:

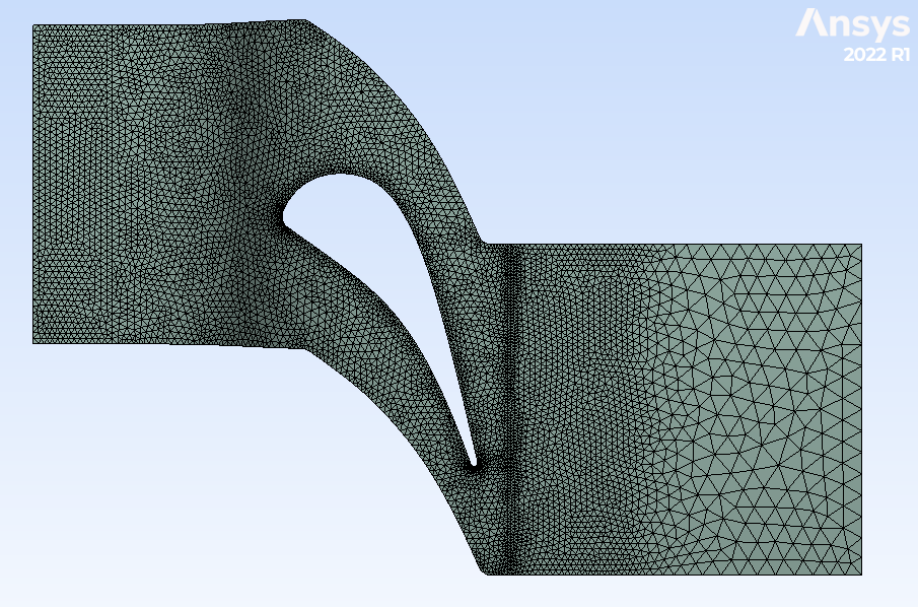

Figure 15: Mesh Example.

The mesh coursing in the last portion of domain is done in order to reduce the number of elements and the computation time, but also to reduce the fluctuations at the outlet region, where some parameters (as Mach number and flow angle) are monitored as output for every iteration done.

The named selection for this project are showed in the following Figure 16:

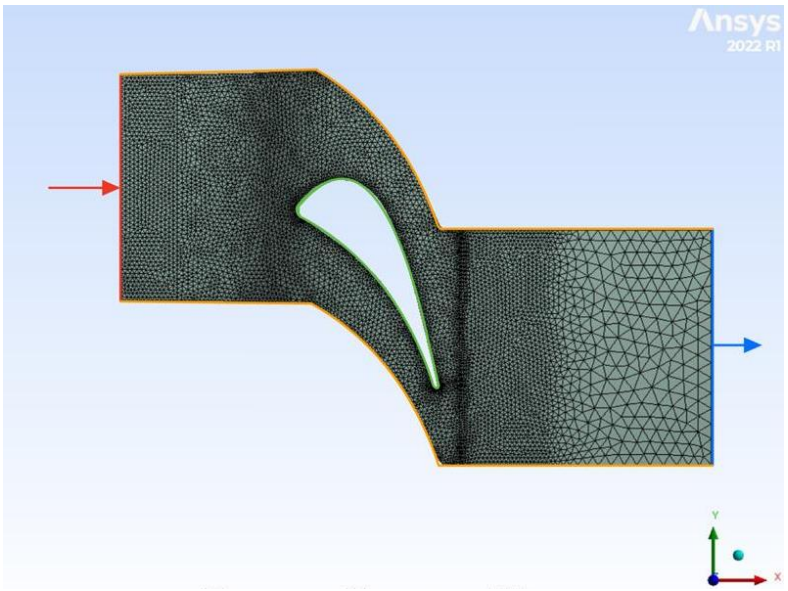

Figure 16: Boundary Conditions: In Red the Inlet; in Blue the Outlet; in Orange the Periodic Boundaries; in Green the Blade Profile;

Referring to Figure 16, In Red is highlighted the Inlet, in Blue the Outlet, in Orange the Periodic Boundaries and in Green the Blade Profile;

Method definition: Simulation Setup

In order to simulate the behaviour of the turbine vane, the following steady state CFX setup is set:

- MAIN SETUP:
  - **Material:** Air Ideal Gas.
  - **Reference Pressure:** 0 atm.
  - **Turbulence Model:** Shear Stress Transport (SST).

- INLET BOUNDARY CONDITIONS:
  - **Inlet Relative Total Pressure (stable):** 161600 Pa.
  - **Inlet Total temperature:** 440 K.

- OUTLET BOUNDARY CONDITIONS:
  - **Outlet Average Static Pressure:** 83289 Pa.

- WALLS BOUNDARY CONDITIONS:
    - **Periodic Walls:** Conservative interface flux.
    - **Interface Model:** Rotational Periodicity.
    - **Blade Walls:** No Slip.
    - All Walls are Adiabatic.

- SIMULATION CONTROL:
    - **Max Iterations:** 250.
    - **Timescale Control:** Auto Timescale.
    - **Length Scale:** Conservative.
    - **Timescale Factor:** 5.
    - **Initialization:** Update from current solution data if possible.

With the mesh size, the Timescale factor influences the Courant number that acts on the accuracy and time of convergence of the residuals and output parameters. With the mentioned Timescale factor and Mesh sizing the optimal number of iteration to be performed is 250.

Method definition: Solution and Results

The Residuals Analysis showed that 250 iterations was an appropriate number to reach convergence, since from 250 to 600 iterations the oscillations decreased in amplitude and the convergence is reached, Figure 34.

In Figure 19 it is reported the monitor of fluid flow angle in output, since this value was highly oscillating for some critical configurations in respect the nominal one. This Output monitor is now converging after 250 iterations, with an oscillation amplitude equal to 0.025°. The Heat Transfer (Figure 17) and the Turbulence (Figure 18) Residuals are showed in the following pages.

The final project that is made of 312 Design Points ran on the Cluster of Politecnico di Torino on 16 parallel processors (HPC PoliTo on Legion) [19]. Every point requires a computational time of about forty minutes.

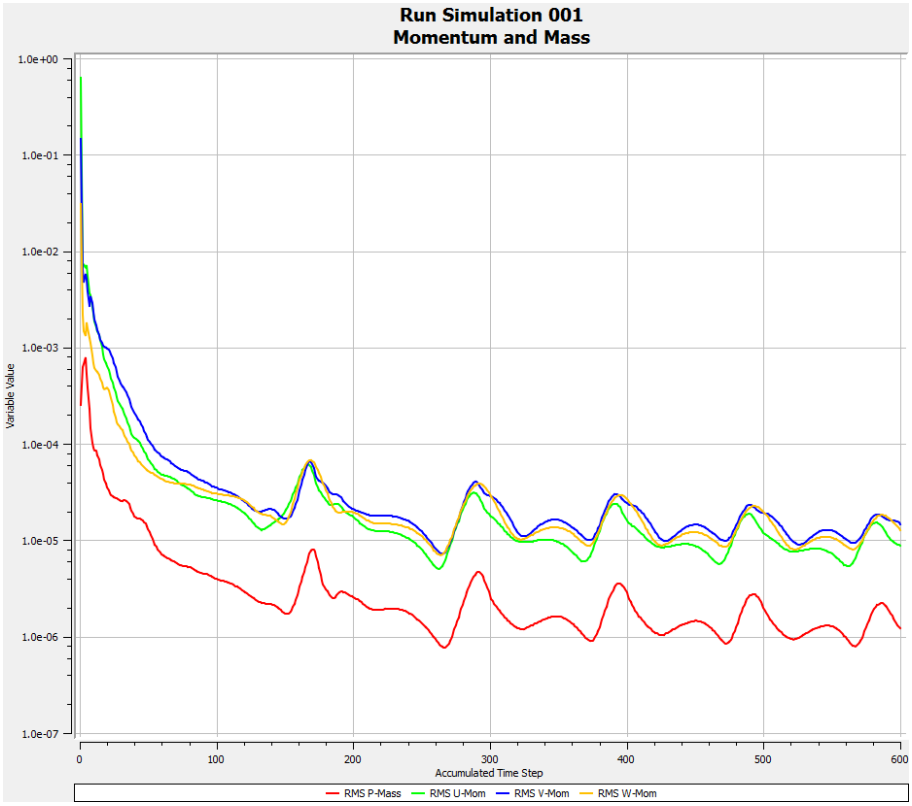

Figure 34: Mass and Momentum Residuals

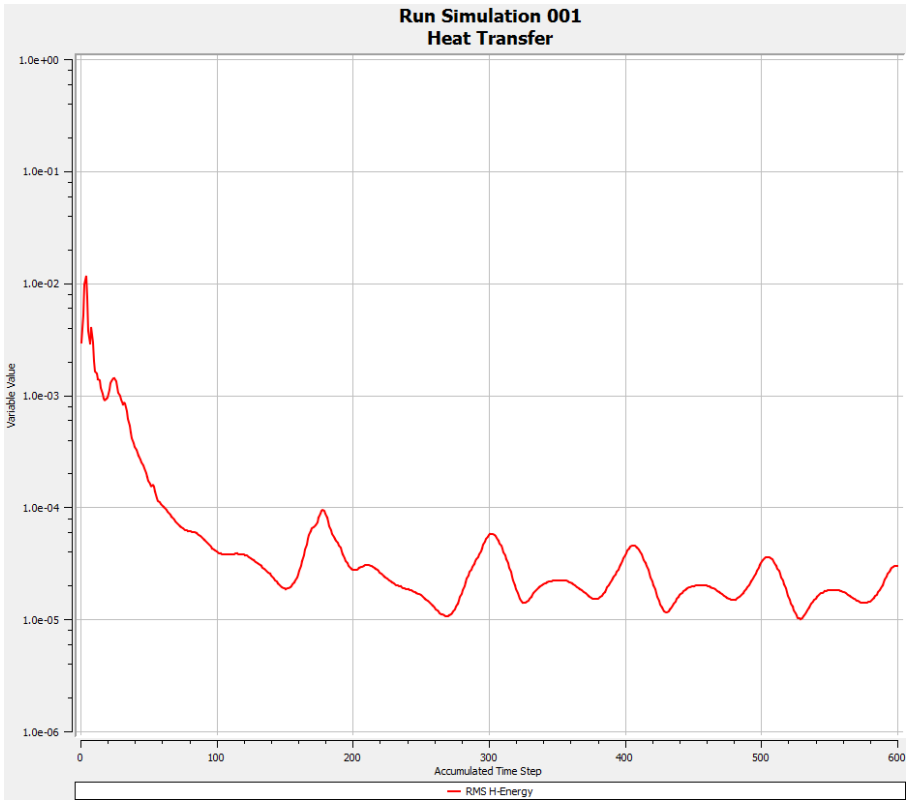

Figure 17: Heat Transfer Residuals

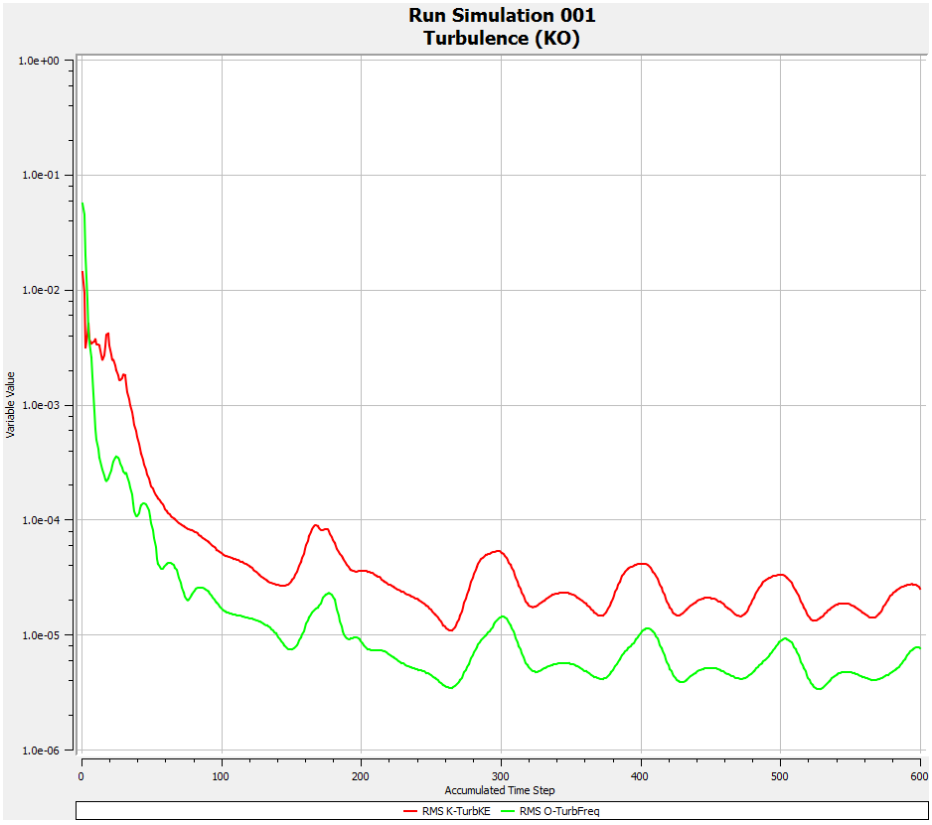

Figure 18: Turbulence Residuals.

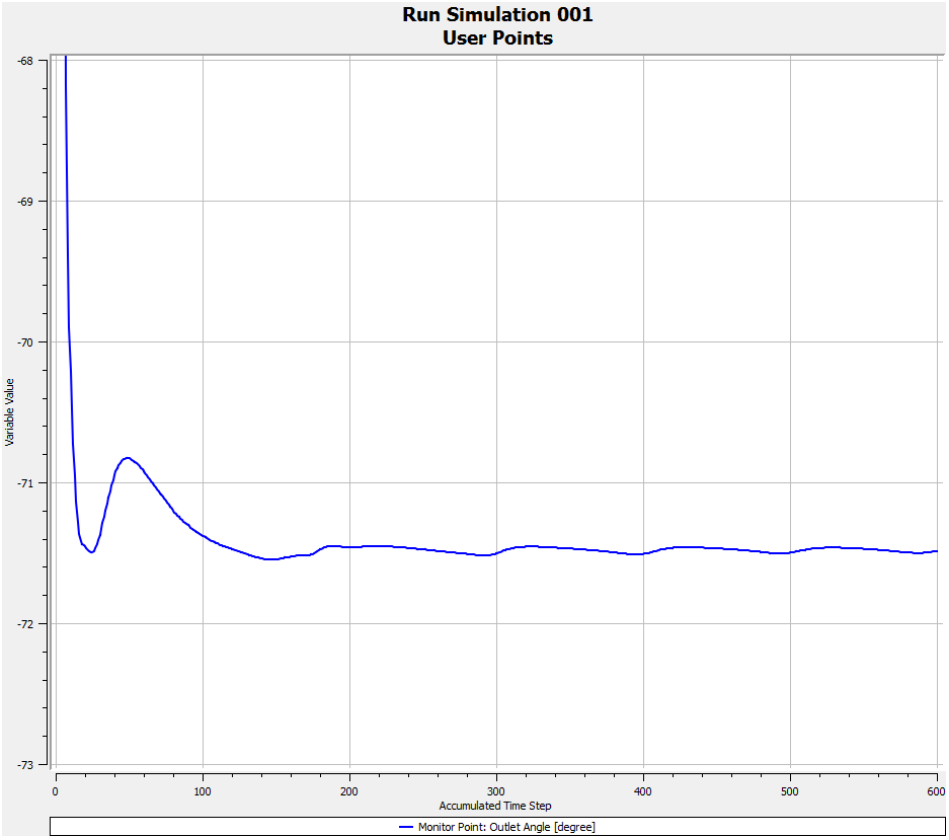

Figure 19: Outlet Flow Angle User Monitor.

Chapter 6:

OPTIMIZATION TECHNIQUES

When analysing a process, experiments are often performed to evaluate which inputs have a significant role and impact on the process output: to reach this aim it is useful to implement a set of actions performed by modelling and optimizing reaction variables thanks to statistical methods. In this paragraph, a brief introduction about the instruments used for this aim is presented, in particular the description of a Design of Experiment and its response surface optimization.

“Optimizing” a configuration means to find the “best” answer of a function or process output, by changing the system’s inputs. This procedure starts from the definition of a Design of Experiment (DOE).

DESIGN OF EXPERIMENT

A Design of Experiment (DOE) is a technique used to determine the location of a certain number of design points, trying to explore the space of input parameters in the most efficient way, or trying to obtain with the minimum number of sampling points the information required. This technique is crucial not only to reduce the number of samples required but also to increase the accuracy of the Response Surface Method (RSM) that will be driven from the results obtained for every design point.

In this research the Latin Hypercube Sampling method is used. Its purpose is to recreate the input distribution through less samples possible. The key of this method consists in the stratification of the input probability distribution: the stratification divides the cumulative curve into equal intervals and for each row and column a single sample is randomly selected. The number of samples is always equal to the number of stratifications [20].

In 2-dimension it’s possible to define a Latin Square if and only if the square grid contains only one sample in each column and each row, as represented in Figure 20. A Latin hypercube is instead the generalisation of this concept to an arbitrary number of dimensions, for which every sample is the only one in each axis-aligned hyperplane containing it.

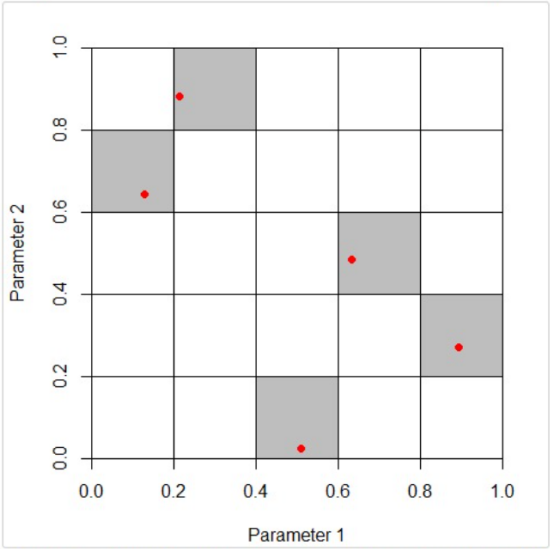

Figure 20: two dimensions of a uniform random Latin Hypercube Sampling Method with 5 samples [20].

The Latin Hypercube Sampling method is an approach that requires to remember in which row and column the sample point was taken, for this reason it requires a certain memory.

RESPONSE SUFRACE METHOD

A Response Surface Method (RSM) is nothing more than a set of statistical techniques and applied mathematics for optimizing experimental models: its goal is to optimize the response affected by several input independent variables.

Originally response surface analysis were applied for modelling experimental responses, but for the aim of this research the methods to model numerical experiments are analysed.

Genetic Aggregation

The method chosen for this Thesis is the Genetic Aggregation Response Surface (GARS) that automates the process of selecting, configuring and generating the various type of response surface that can best suit to each output parameter in the problem. GARS automatically builds the RS type that is the most appropriate approach for each output between the different types of RS available (Full 2nd order Polynomial, Non-Parametric Regression, Kriging, and Moving Least Squares), [21].

GARS normally takes more time in respect the other techniques, because it solves multiple RS and cross-validation process, but in general is more reliable than classical models. To select the best possible RS, a genetic algorithm that takes into account both accuracy and stability of the RS is used.

According to [23] the GARS can be written as an ensemble using a weighted average of different meta-models:

$$y_{ens}(x) = \sum_{i=1}^{N_M} w_i \, y_i(x) \tag{42}$$

Where:

- y_{ens} is the prediction of the ensemble;
- y_i is the prediction of the i-th response surface;
- N_M is the number of metamodels, higher or equal to 1;
- w_i is the weight factor of the i-th response surface;

The weight factor has to satisfy the following requirement:

$$\sum_{i=1}^{N_M} w_i = 1 \;\; and \; w_i \geq 0, 1 \leq i \leq N_M \tag{43}$$

To estimate the best weight factors, DesignXplorer minimizes the Root Mean Square Error (RMSE) of the DOE samples on y_{ens}' and the ones of the same design points based on the cross-validation of $y_{ens}(PRESS_{RMSE})$:

$$RMSE(y_{ens}) = \sqrt{\frac{1}{N}\sum_{j=1}^{N}\left(y(x_j) - y_{ens}(x_j)\right)^2} \tag{44}$$

$$PRESS_{RMSE}(y_{ens}) = \sqrt{\frac{1}{N}\sum_{j=1}^{N}\left(y(x_j) - y_{ens,-j}(x_j)\right)^2} \tag{45}$$

With

$$y_{end,-j}(x) = \sum_{i=1}^{N_M} w_i \, y_{i,-j}(x) \qquad (46)$$

Where:

- x_j is the j-th design point:
- $y(x_j)$ is the output parameter value at x_j;
- $y_{i,-j}$ is the prediction of the i-th response surface built without the j-th design point;
- N is the number of design points;

A brief introduction to the meta-models implemented by the GARS is presented.

Full 2nd-Order Polynomials

The Full 2nd - Order Polynomials is a Response Surface Method based on a Central Composite Design (CCD) DOE, then for our set of samples, defined starting from a Latin Hypercube Method, it is not possible to be analysed with this model. For a sake of completeness the method is described below.

This analysis assumes a total of n sampling points and every point has a corresponding known output value. Based on these samples a regression analysis determines the relation between input and output parameters. The regression model is based on a 2nd order polynomial and is generally an approximation of the true input-to-output relation. The RS is the resulting approximation of the output parameters in respect the input variables.

According to [22] this method performs the following steps in order to select the best RS:

- Scaling on input parameters.
- Transformation on input parameters.
- Calculation of polynomial coefficients based on these modified input values. Some polynomial terms can be filtered by using the F-Test filtering and Significance Level properties.
- Back-transformation on the output parameter.
- Back-scaling on the output parameter, Figure 21:

$$X \xrightarrow{scaling} X\_scal \xrightarrow{transformation} X\_trans \xrightarrow{regression\ model} Y\_trans \xrightarrow{back\ transformation} Y\_scal \xrightarrow{back\ scaling} Y$$

Figure 21: scheme of Back-scaling on Output Parameters [22].

As a consequence, the generated RS can fit more complex responses in respect simple parabolic curvatures.

Kriging

This is a meta-modelling algorithm that provides an improved response quality and fits higher order variations of the output. It combines a polynomial model similar to the standard RS with local deviations by a multidimensional interpolation. This model does not supports any discrete parameter and its effectiveness is based on the ability of its internal error estimator to increase RS quality thanks to the generation of refinement points and their addition to the areas of the RS most in need of improvement.

Kriging offers an option of auto-refinement: it automatically updates the refinement points during the RS update.

$$PredictedRelativeError = \frac{100\ PredictedRelativeError}{O_{max} - O_{min}} \quad (47)$$

Where O_{max} and O_{min} are the maximum and minimum known values (on design points) of the output parameter.

Non-Parametric Regression

Non-Parametric Regression (NPR) is a procedure that is initialized with one of the available DOE types and is implemented in DesignExplorer to predict highly nonlinear behaviour of the outputs in respect the inputs. It belongs to a class of techniques called "Support Vector Method" (SVM) that uses hyperplanes to categorize a subset of input sample vectors, considered as sufficient to represent the output in question (support vector set). A compromise between accuracy and computational speed is the criteria in order to determine the values. The NPR is only used for problems where low order polynomials do not dominate [22].

OPTIMIZATION METHOD:

In this section are analysed various optimization methods to achieve a targeted objective or goal (Goal Driven Optimization).

Screening

This first analysed method is the default one and can be used both for Direct Optimization systems and Response Surface Optimization; it allows to generate new samples and organize them on the base of objectives and constraints. All input parameters can be valid for this kind of non-iterative method: typically is used for a preliminary design [25].

An important constraint for this method is that the number of samples to generate for the optimization has to be greater than the number of enabled input parameters.

MOGA (Multi-Objective Genetic Algorithm)

The MOGA (Multi-Objective Genetic Algorithm) allows to generate a new sample set or use an existing set for providing a more refined approach than the Screening method [26]. MOGA can also handle multiple goals and for this reason this method has been chosen to carry the analysis of the previous Thesis [13].

The method supports all kind of inputs and consists of the following steps:

1. An initial population is used to run MOGA;
2. MOGA generates a new population thanks to a cross-over and a mutation;
3. The design points in the new population are updated;
4. The optimization is validated for convergence with ‘yes’ (Optimization converged) or ‘no’ (Optimization Not converged);
5. If the optimization didn’t converged, it is validated for fulfillment of stopping criteria: if the stopping criteria have not been met, MOGA is run again to generate a new population, starting again with the procedure from Step 2;
6. In conclusion steps from 2 to 5 are repeated in sequence until the optimization has converged or the stopping criteria has been met; if either of these things occurs, the optimization is ended;

NLPQL (Nonlinear Programming by Quadratic Lagrangian)

This method [27] solves constrained nonlinear programming problems that minimize $f(\{x\})$ subject to:

$$g_k(\{x\}) \leq 0, \forall\, k = 1,2,\dots,K \qquad (48)$$

$$h_l(\{x\}) = 0, \forall\, k = 1,2,\dots,L \qquad (49)$$

Where:

$$\{x_L\} \leq \{x\} \leq \{x_U\} \qquad (50)$$

The assumption that objective functions and constraint are continuously differentiable is done. The aim of this method is to create a sequence of quadratic programming subproblems that are found by a quadratic approximation of the Lagrangian function and the linearization of constraints. This kind of approach works for low-scale and well-scaled problems and its accuracy depends on the gradient's accuracy: it is necessary that numerical based gradients, that are finite difference based, are as accurate as possible, since analytical gradients are unavailable for most practical problems [27].

The NLPQL method is a derivation of the Newton method that is briefly described in this section:

If $f(x)$ is a multivariable function and can be expanded in Taylor's series about point x, then:

$$f(x+\Delta x) \approx f(x) + \{\Delta x\}^T\{f'(x)\} + \left(\frac{1}{2}\right)\{\Delta x\}^T[f''(x)]\{\Delta x\} \qquad (51)$$

The assumption that Taylor series models a local area of the function by a quadratic approximation is done. Another assumption is that at the end of every iterative cycle, the Equation (51) would be exactly valid.

$$\Phi(\Delta x) = f(x+\Delta x) - (\{f(x)\} + \{\Delta x\}^T\{f'(x)\} + \left(\frac{1}{2}\right)\{\Delta x\}^T[f''(x)]\{\Delta x\}) \qquad (52)$$

The first variation of Equation (52) with respect to Δx has to be equal to zero, then:

$$f(x+\Delta x)_{,\Delta x} - (\{f'(x)\} + [f''(x)]\{\Delta x\}) = 0 \qquad (53)$$

Since the variation of the converged solution with respect to the increment in the independent variable vector has to be equal to zero, the Equation (53), where j indicates the iteration, can be written as the following:

$$\{x_{j+1}\} = \{x_j\} - [f''(x_j)\}^{-1}\{f'(x_j)\} \quad (54)$$

This conclusion is done because the converged solution does not depend on the length of the step. Equation (54) is used in the main quadratic programming scheme.

For what concerns the NLPQL derivation, a single-objective nonlinear optimization problem is considered with the assumption that it is smooth and analytic throughout, with N decision variables.

Considering Equation (48) and Equation (49), L and K are the numbers of inequality and equality constraints. In order to make an approximation of the quadratic subproblem, the assumption of only equality constraint is done [27].

Mixed-Integer Sequential Quadratic Programming (MISQP)

MISQP (Mixed-Integer Sequential Quadratic Programming) is an optimization algorithm based on mathematical methods that are solving Mixed-Integer Non-Linear Programming (MINLP) [28]:

1. Two continuously differentiable functions in all $x \in \mathbb{R}^{n_c}$: f(x,y) and g(x,y) are given;
2. f(x,y) is minimized subject to $g_j(x,y) = 0. j = 1, \ldots . m_e$ and $g_j(x,y) \geq 0. j = m_e + 1, \ldots, m$, where $x \in \mathbb{R}^{n_c}$, $y \in \mathbb{N}^{n_c}$, $x_l \leq x \leq x_u$, $y_l \leq y \leq y_u$

The quantities x and y are intended respectively as vectors of the continuous and integer variables, while the problem functions $f(x,y)$ and $g_j(x,y)$, j=1,…,m are continuously differentiable for every $x \in \mathbb{R}^{n_c}$. The problem functions are calculated only at integer points and never at any fractional value in between.

The method is made of a constraint linearization and the construction of a quadratic approximation of the Lagrangian function, later mixed-integer quadratic programs are generated and solved by an efficient branch-and-cut method. Mixed-Integer Sequential Quadratic Programming can also solve non-convex nonlinear mixed-integer programs [28].

Chapter 7

Introduction to Optimization Analysis

During the analysis discussed in Chapter 6, many Response Surface and Optimization methods are described in order to apply different criterion to the optimization of a HPT vane profile. In the following Chapter the methods described are used for the definition of 3 candidate Design Points that might satisfy as much as possible the condition of maximizing the efficiency or minimizing the Angle Coefficient.

The Goal of the research is to maximize the vane's efficiency, by maintaining the Angle Coefficient, as much as possible equal to zero. In Chapter 2 the Equation (2) and Equation (5) define respectively the Efficiency and the Angle Coefficient of the Vane.

Nominal Configuration Evaluation

The Nominal Vane analyzed in Chapter 2 is simulated in order to obtain a valid comparison with the results obtained from the optimization procedure. The candidates found in order to achieve the maximum possible efficiency are compared with the following baseline in Figure.

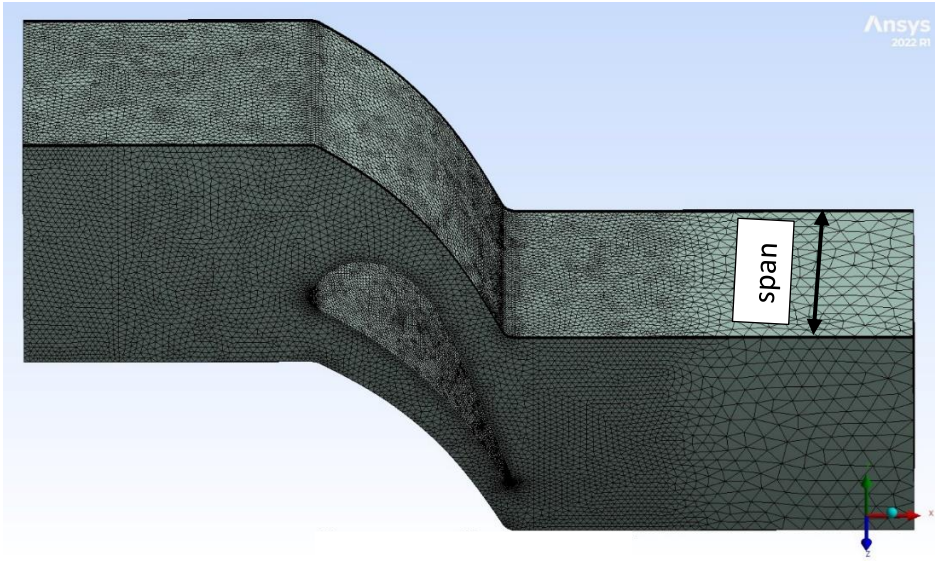

Figure 40: Mesh of Nominal Profile.

The height of the Stator Vane, equal to the Span, is found thanks to the following [29] documentation.

This height is Constant, as mentioned in Chapter 2, while the nominal number of vanes is equal to 43 and will not change for all the optimization procedure.

Since the Endwall's height is kept constant, the fluid separation can only be attributed to Horseshoe Separation, due to the presence of the Blade and not to the divergence of the channel, as happens to every Optimized Configuration. For this reason it is expected that the Nominal Vane's Efficiency is going to be slightly higher in respect the optimized ones, but with different operating conditions in respect the Design point of the Optimized Profiles.

The 18 Nominal Input Parameters are reported in Table 6 and are referring to the B-Spline control points in Figure 41:

Table 6: Input Parameters for Nominal Case.

Parameter Name
P1 - x0_SS (mm)
P2 - x1_SS (mm)
P3 - x2_SS (mm)
P4 - x3_SS (mm)
P5 - x4_SS (mm)
P6 - x2_PS (mm)
P7 - y0_SS (mm)
P8 - y2_SS (mm)
P9 - y3_SS (mm)
P10 - y4_SS (mm)
P11 - y0_PS (mm)
P12 - y1_PS (mm)
P13 - y2_PS (mm)
P14 - x0_DIFF (mm)
P15 - x1_DIFF (mm)
P16 - x2_DIFF (mm)
P17 - x3_DIFF (mm)
P18 - Stagger_angle (degree)

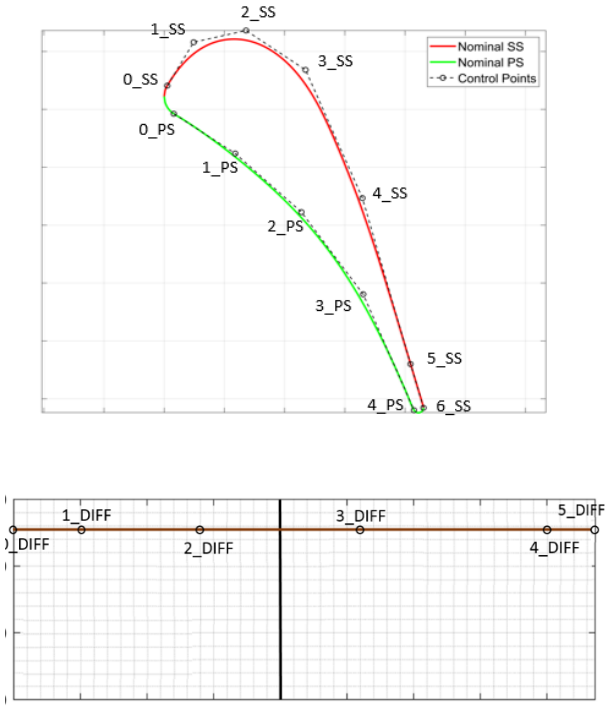

Figure 41: Scheme of Control Points for Vane and Endwalls for Nominal Case.

With the same setup used to run the Optimization, the Nominal Configuration has been tested: the following output parameters are obtained in Table 7 and are referring to the two Sections reported in Figure 42:

Table 7: Output Parameters for Nominal Conditions

Parameter Name
P19 - Angle Losses
P20 - Exit Angle (degree)
P21 - Inlet Mass Flow (kg s^-1)
P22 - Outlet Mass Flow (kg s^-1)
P23 - Outlet Mach
P24 - Inlet Mach
P25 - Outlet Static Pressure (Pa)
P26 - Outlet Static Temperature (K)
P27 - Outlet Pressure (Pa)
P28 - Outlet Total Temperature (K)
P29 - Outlet Vel (m s^-1)
P30 - Stator Losses
P31 - Stator Efficiency

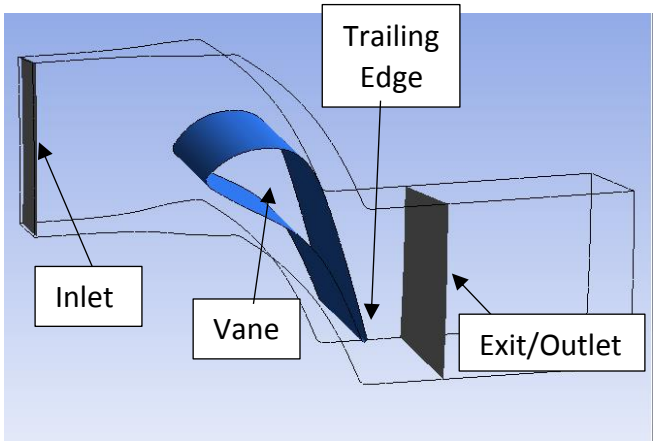

Figure 42: Named Sections where the Output Parameters are evaluated.

All the quantities are evaluated as Mass Flow Average on the corresponding Inlet or Outlet/Exit sections that are respectively 1 mm far from the domain inlet and half an axial nominal chord far from the Trailing edge. Only the Outlet Static Pressure is evaluated as Area Average on the Outlet section.

The Flow Fields are reported in the following images: in Figure 43 is reported the Mach Number Contour at mid-span while Figure 44 shows the Total Pressure Contours.

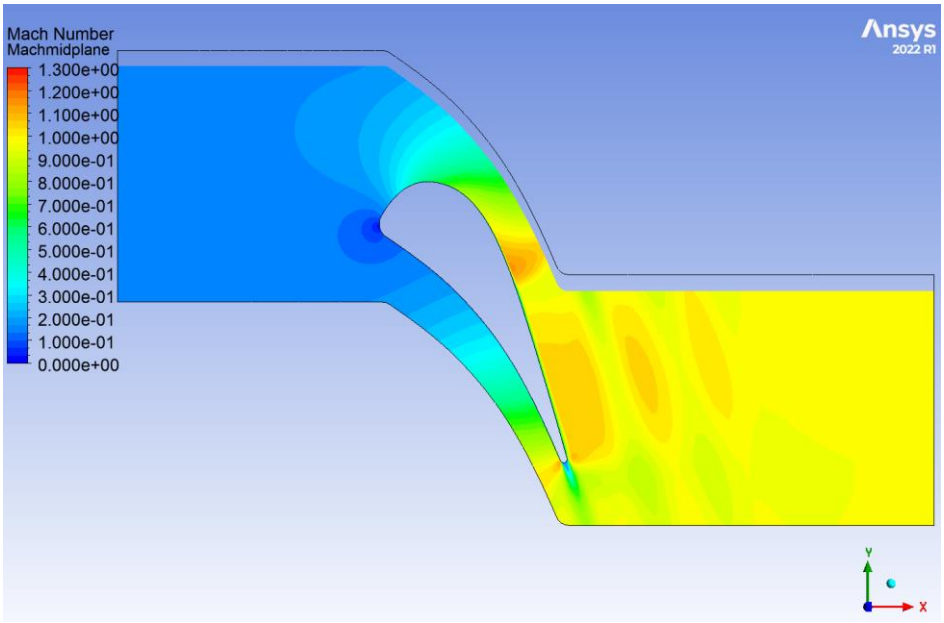

Figure 43: Mach Number Contour for Nominal Case

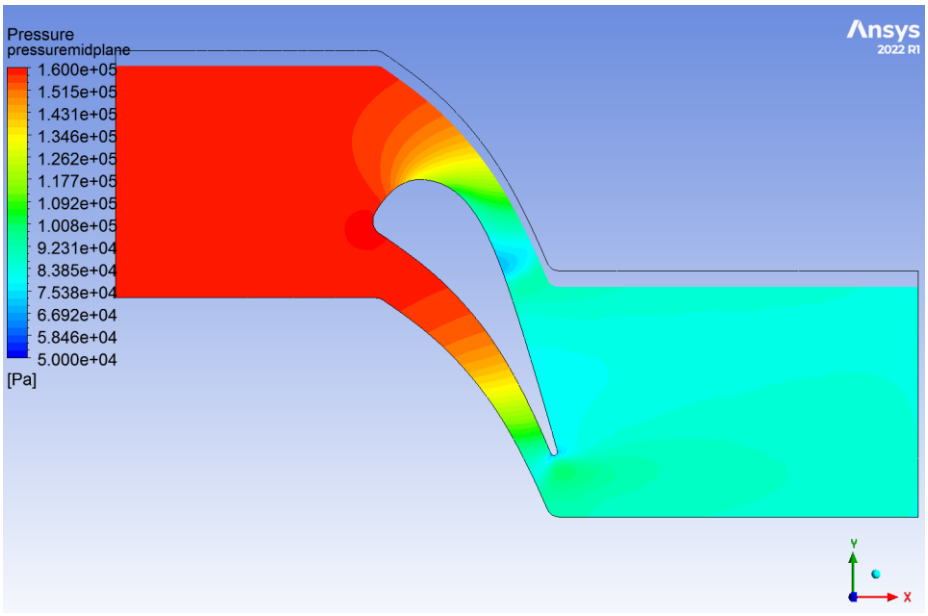

Figure 44: Total Pressure Contour for Nominal Case 22

In Figure 45 instead is showed the Velocity Vector Distribution at mid-span plane in order to highlight the fact that no recirculation zones are present:

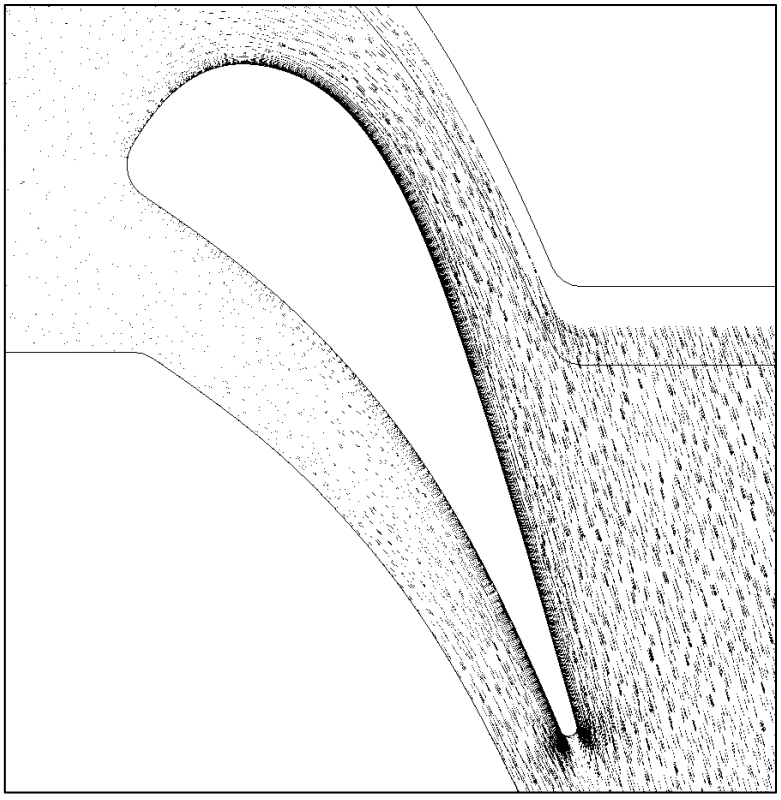

Figure 45: Velocity Vector Distribution for Nominal Case.

It is useful to generate an iso-volume with the Lambda-2 criterion that identifies the vortices from a three dimensional fluid velocity field [30]. The Lambda-2 method determines if a point of a fluid domain is a part of a vortex core: a vortex is defined as a connected region for which every point in this region is a part of a vortex core.

In the following Figure 46 are reported the vorticities detected with Lambda-2 method on the Nominal profile: the colors are indicating the Turbulence Kinetic Energy of the vortices.

It is important to notice that since the endwall's span is not changing, all the turbulences present are due to the Horseshoe effect. In Figure 46: isovolume of Lambda-2 criterion for Nominal Case. it is also possible to distinguish between the vortices coming from the Pressure Side and the ones coming from the Suction Side.

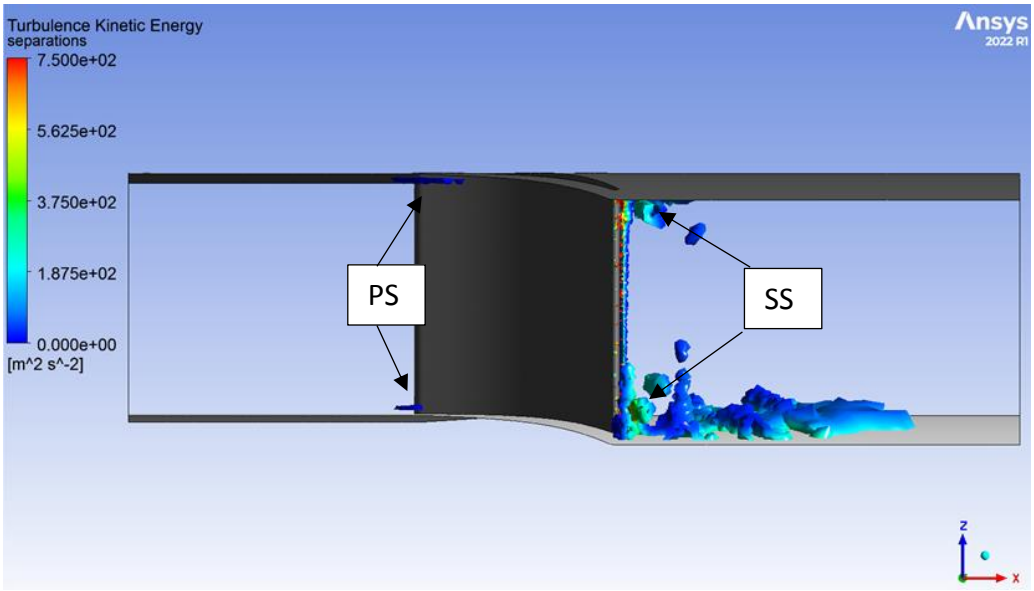

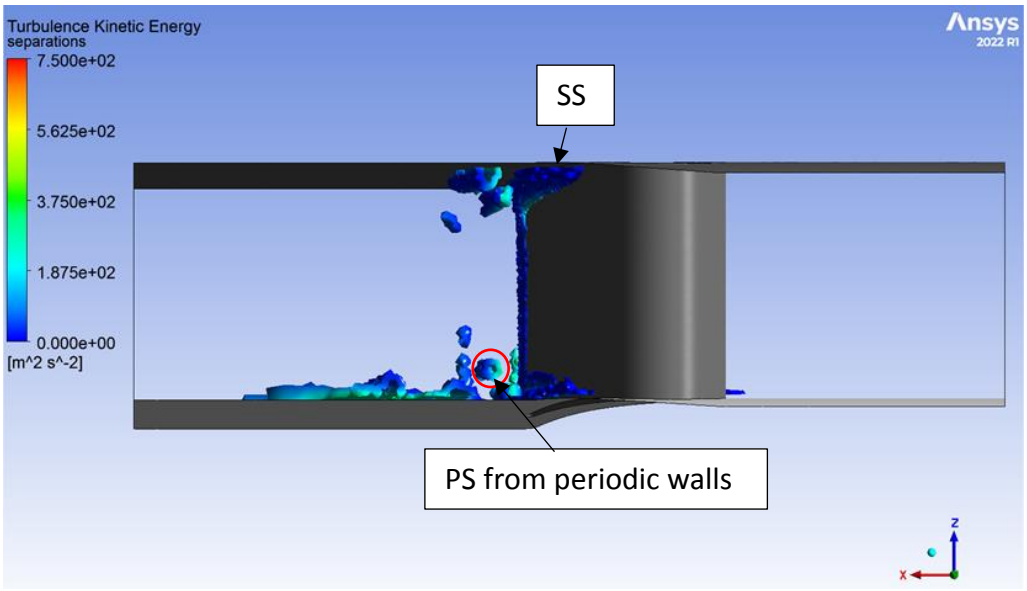

Figure 46: isovolume of Lambda-2 criterion for Nominal Case.

Response Surface Analysis

The First Response Surface method that is analyzed is the Genetic Aggregation Response Surface Method that has been previously analyzed in Chapter 6.

The Method is performed starting from all the 18 input and 13 output parameters but only the Efficiency and the Angle Coefficient in Output are considered during this study.

First of all, the Local Sensitivity Analysis is performed, for both Efficiency and Angle coefficient. The results of the analysis are reported in the following Figure 47 and Figure 48.

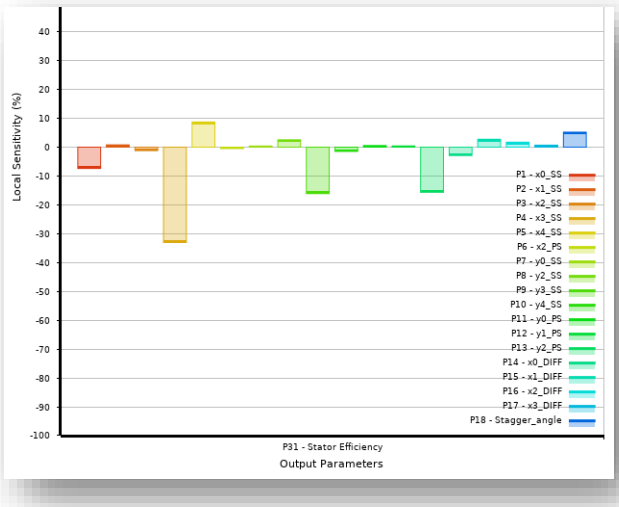

Figure 47: Local Sensitivity Analaysis for GA, Efficiency.

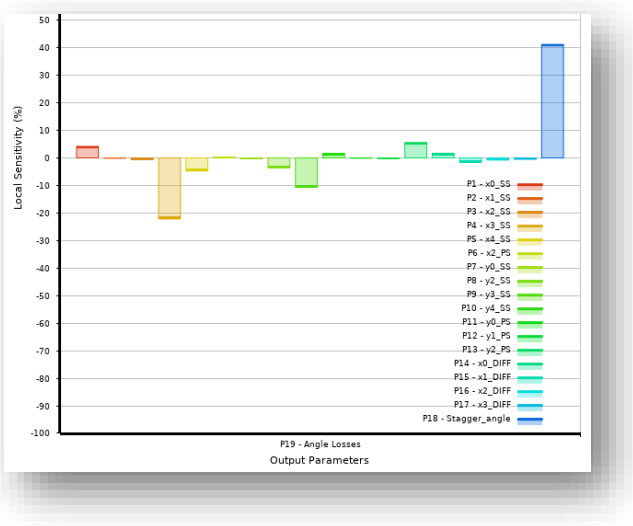

Figure 48: Local Sensitivity Analaysis for GA, Angle Coefficient.

For the Angle Coefficient it is clear that the Stagger Angle has the highest influence on the results, since higher is its value, higher will be the value of Angle Coefficient (as mentioned in Chapter 2). The point 4 on the Suction Side (see Figure 26), instead, is the Point that affects the most the behavior of the stage in terms of both Efficiency and Angle Coefficient. For these reasons, below are reported the two Response Surfaces for Efficiency (Figure 49) and Angle Coefficient (Figure 50) (on z-axis), with the two most influent input parameters: x and y of point 3 on suction side for the first case, while stagger and x of point 3 on suction side for the second case.

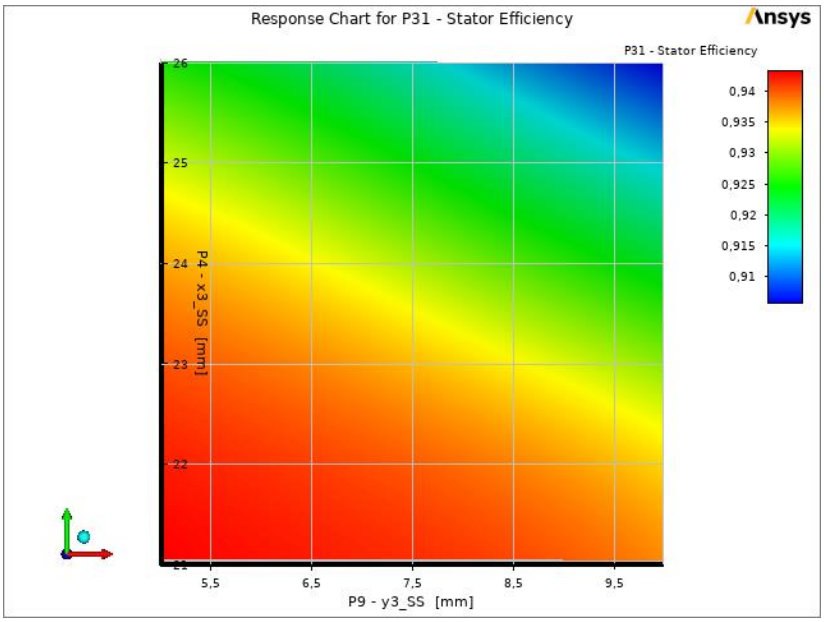

Figure 49: Efficiency Response Surface in respect X3_ss and Y3_ss

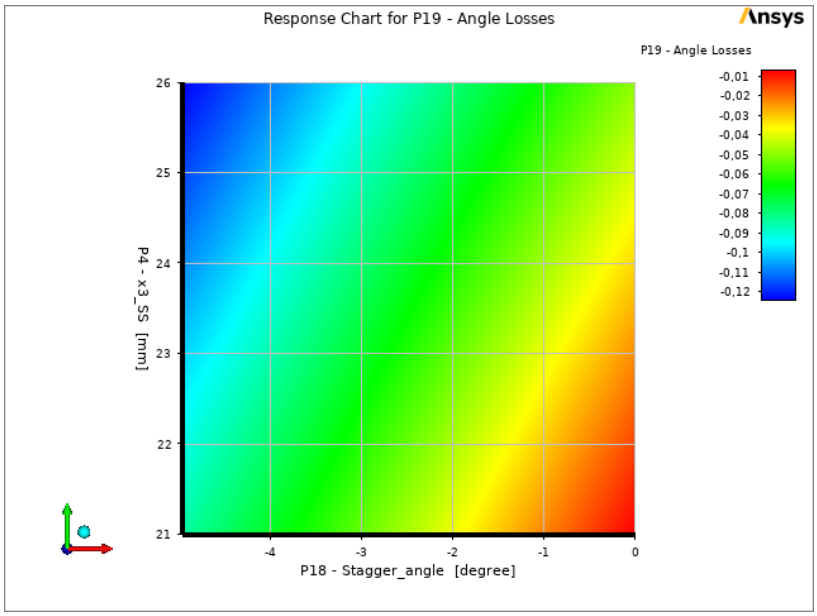

Figure 50: Angle Coefficient Response Surface in respect Stagger Angle and X3_ss

From Figure 49 it is possible to see the influence of the point 3 on the suction side in respect of the Efficiency.

By moving the point downward and to the left of around 5 mm for every direction it is possible to detect an increase in Efficiency from 90% to around 94.5%.

From Figure 50 instead, it is possible to see how an increase in stagger angle leads to an increase of the absolute value of the Angle Coefficient, which target is its zeroing.

Optimization Methods: Best Candidates

In this paragraph the results of some optimization methods performed starting from the Genetic Aggregation RS showed in Chapter 6 are reported and compared with the Nominal Configuration. The following 4 methods are used in order to optimize the stator configuration in terms of Efficiency and/or Angle Coefficient, described in Chapter 2:

1. Screening Optimization to maximize Vane's Efficiency;
2. MISQP Optimization to maximize Vane's Efficiency;
3. NLPQL Optimization to maximize Vane's Efficiency;
4. MOGA Optimization to maximize Vane's Efficiency and to seek Zero Angle Coefficient;

Before analyzing in detail every result, a brief comparison between the generated profiles is performed in Figure 51:

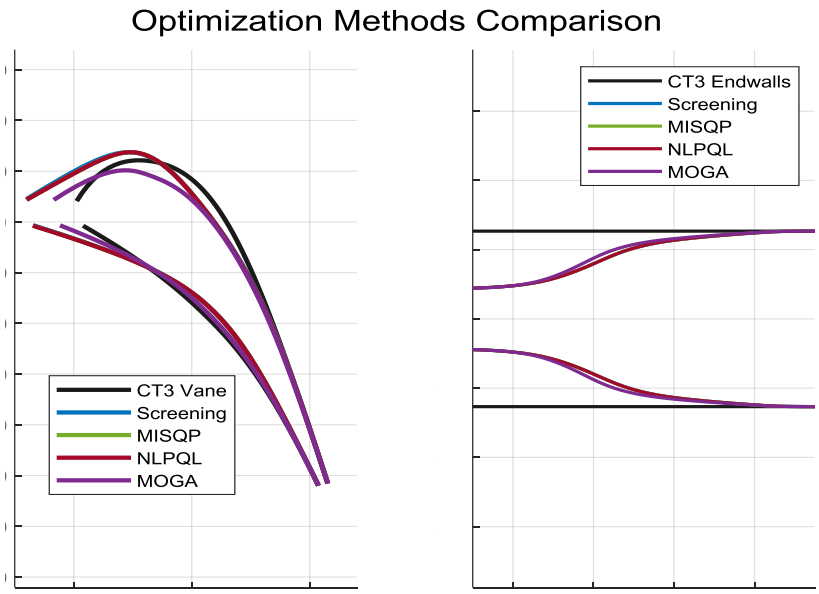

Figure 51: Optimal and Nominal Configuration Comparison

From Figure 51 it is clearly visible that MISQP and NLPQL methods are giving exactly the same geometry results for both vane end endwalls, while Screening Optimization's vane is very close to the previous.

In Table 8 are reported the input parameters of the 5 configurations showed as percentage of the Nominal Condition:

Table 8: Input Parameters Comparison for different Methods

Method Name:	Nominal Condition	GA-Screening	GA-MOGA	GA-MISQP	GA-NLPQL
P1 - x0_SS (%)	100.000	19.135	62.891	19.135	19.135
P2 - x1_SS (%)	100.000	45.711	139.000	69.993	69.993
P3 - x2_SS (%)	100.000	81.062	95.482	81.062	81.062
P4 - x3_SS (%)	100.000	89.464	89.784	89.464	89.464
P5 - x4_SS (%)	100.000	100.872	99.846	100.654	100.654
P6 - x2_PS (%)	100.000	109.731	101.258	109.731	109.731
P7 - y0_SS (%)	100.000	109.863	105.688	106.274	106.274
P8 - y2_SS (%)	100.000	124.706	69.401	124.706	124.706
P9 - y3_SS (%)	100.000	73.438	74.552	73.438	73.438
P10 - y4_SS (%)	100.000	97.879	99.625	99.258	99.258
P11 - y0_PS (%)	100.000	85.858	90.413	100.068	100.068
P12 - y1_PS (%)	100.000	98.279	92.964	98.115	98.115
P13 - y2_PS (%)	100.000	87.352	92.834	87.443	87.443
P14 - x0_DIFF (%)	100.000	90.043	96.393	90.043	90.043
P15 - x1_DIFF (%)	100.000	109.870	94.314	109.870	109.870
P16 - x2_DIFF (%)	100.000	108.485	92.422	108.485	108.485
P17 - x3_DIFF (%)	100.000	109.524	108.328	107.580	107.580
P18 - Stagger_angle (degree)	0.000	-0.003	-0.115	0.000	0.000

While in Table 9 are reported the results of Mass Flow, Inlet Mach and Angle Coefficient in respect of the Nominal Profile and of Efficiency and Root Square Index Results:

Table 9: Output Parameters Comparison for different Methods

Method Name:	Mass Flow Ratio [/]	Inlet Mach Number Ratio	Angle Coefficient Ratio	Efficiency [%]:	Root Square Index [%]:
GA-Screening	1.024	3.598	0.577	95.58%	7.55%
GA-MISQP	1.030	3.631	0.5416	95.57%	7.19%
GA-NLPQL	1.030	3.630	0.5429	95.56%	7.20%
GA-MOGA	1.007	3.503	-0.0088	94.03%	9.71%
Nominal Profile	1.000	1.000	1.0000	96.16%	73.84%

Where the Root Square Index is created in order to define which profile better follows the design conditions of:

- Nominal Mass Flow rate equal to the Baseline (Nominal Condition);
- Inlet Mach Number equal to 0.6 (as already discussed in Chapter 2);
- Seek zero Angle Coefficient (to have a flow angle parallel to metal angle);
- Maximize efficiency;

The relation used to obtain the Root Square Index value of the i-th method is the following:

$$Root\ Square\ Index = \sqrt{\left(\frac{\dot{m}_i - \dot{m}_{Nom}}{\dot{m}_{Nom}}\right)^2 + \left(\frac{M_i - 0.6}{0.6}\right)^2 + \left(\frac{\alpha_i - \alpha_{Nom}}{\alpha_{Nom}}\right)^2 + \left(\frac{\eta_i - 1}{1}\right)^2} \quad (55)$$

For the Nominal Stator, the Root Square value is high because the inlet Mach number is much lower than the other candidates.

The optimization is performed in order to have the maximum possible efficiency with an inlet Mach Number that is around 0.6: for this reason the Inlet Mach is an important quantity to be considered during all analysis.

From the results reported in Table 9 it is possible to deduce that the MISQP method has the best possible compromise between the parameters. In order to verify this assumption, in the next paragraphs are analyzed in detail the results of each method .

Screening Optimization Method Results

The Screening Optimization Method generated three candidates from which the best one in terms of maximum verified efficiency has been picked: in the following Figure 52 it is reported the Mach Number Contour at Midspan:

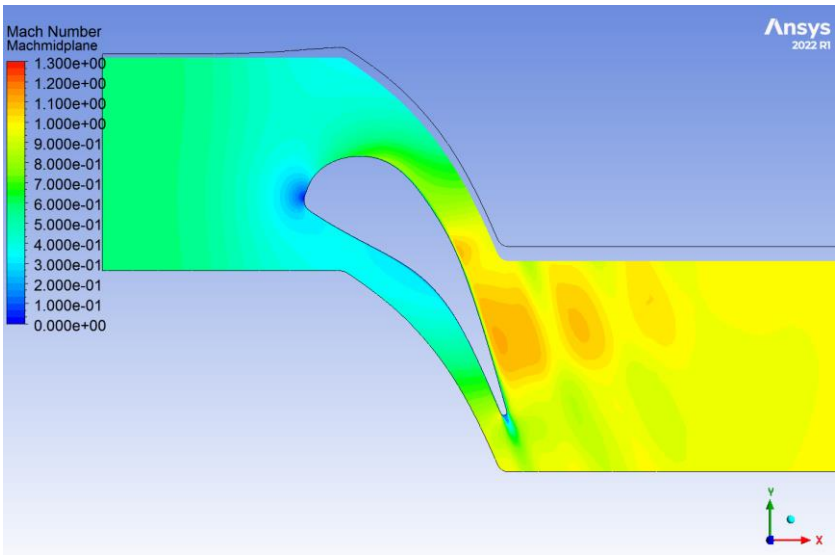

Figure 52: Mach Number Contour for Screening Optimization.

In a different way in respect the Nominal Profile in Figure 53, the shock wave where the fluid reaches supersonic conditions is located more on the Trailing Edge portion.

In Figure 53 it is represented the Midspan Total Pressure Contour.

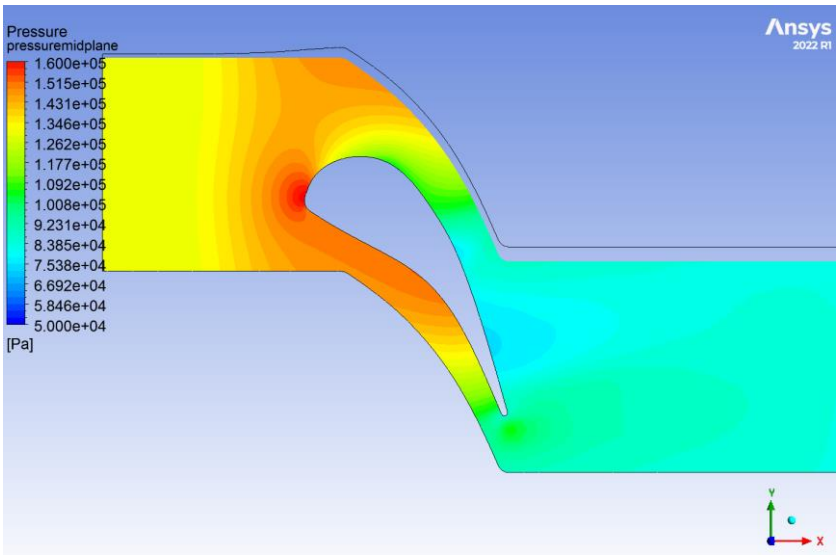

Figure 53: Total Pressure Contour for Screening Optimization.

As done for the Nominal CT3 Stator, the Lambda-2 criterion is used to determine and visualize the presence of turbulences due to separations and Horseshoe Vortex: in the following case a diverging endwall is considered and for this reason it is possible to detect separations due to the divergence of the flow.

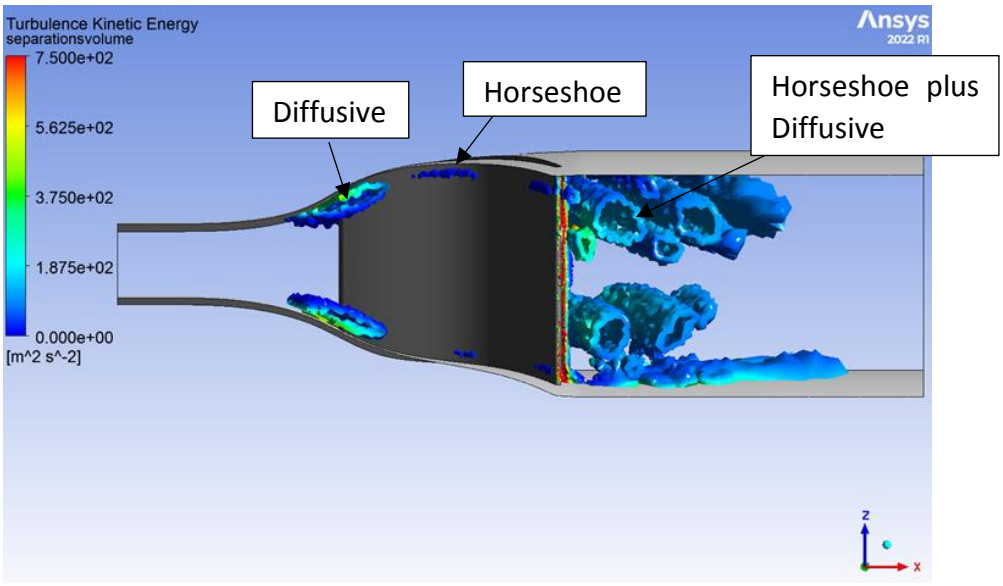

Figure 54: Lambda-2 Method for Screening Optimization.

These diffusive bubble are indicated in Figure 54. The Horseshoe Vortices are significantly enlarged in respect the Nominal Case because they are combined with the diffusive bubbles: The intensity of the turbulence has increased starting from the perturbation due to the presence of diffusive bubbles.

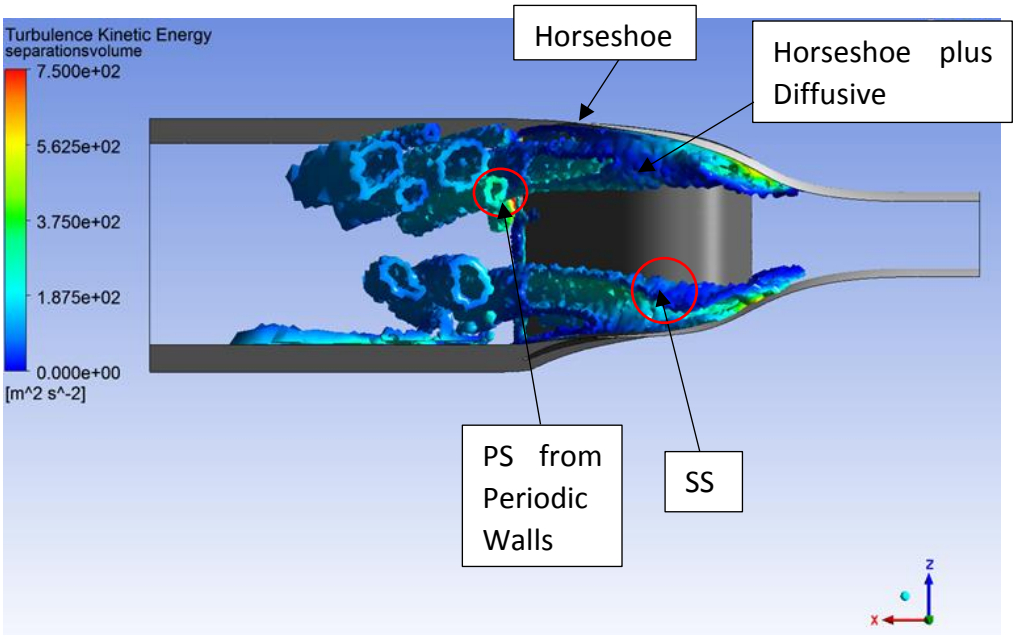

Figure 55: Lambda-2 Method for Screening Optimization.

In Figure 55 it is clearly visible how the SS vorticity highlighted in red starts from the separation volume in the diverging part of the blade. It is possible to see also some Vortices coming from the Pressure Side, with a lower intensity in respect of the one coming from the Suction Side SS.

MISQP Optimization Method Results

The following configuration presents the best compromise between all the design outputs: its configuration is very similar to the configuration optimized with the Screening Method with some small differences on the Leading Edge Suction Side. Therefore the results are similar to the one discussed in the previous paragraph.

In Figure 56 and Figure 57 are reported the Mach Number and Total Pressure contour at midspan.

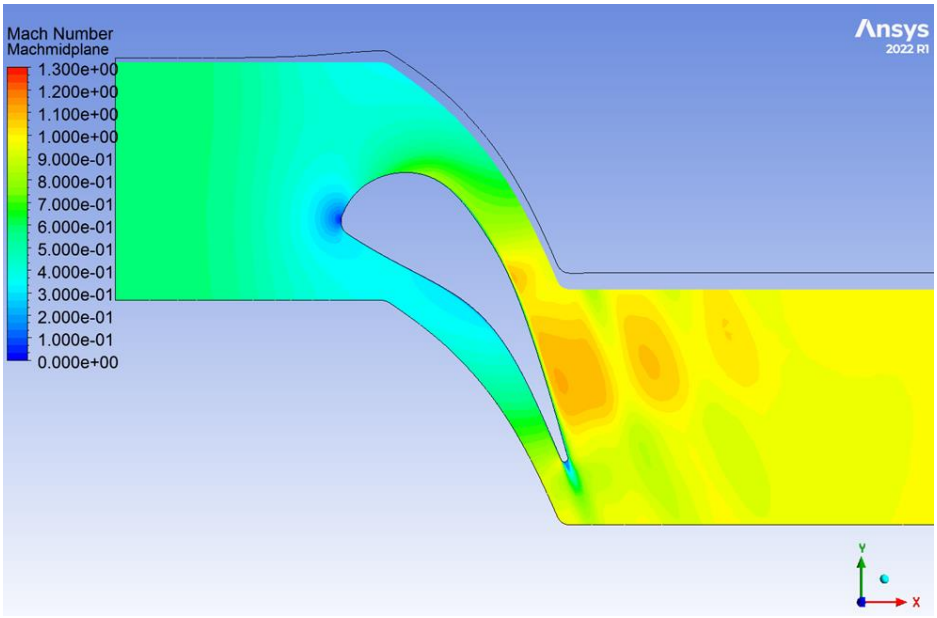

Figure 56: Mach Number Contour for MISQP Optimization.

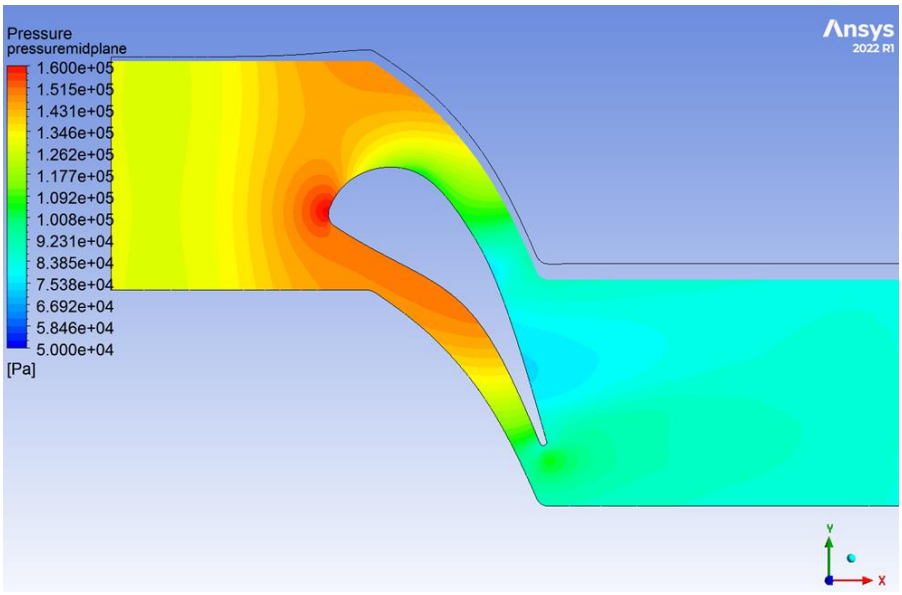

Figure 57: Total Pressure Contour for MISQP Optimization.

For what concerns the vorticity, this configuration shows a slight increment in the Horseshoe Vortex on the Pressure Side near the Hub, as shown in Figure 58:

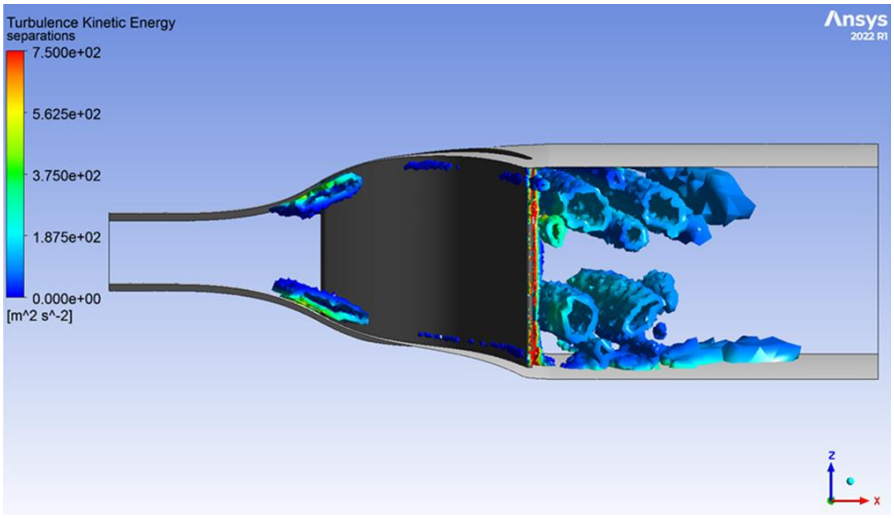

Figure 58: Lambda-2 Method for MISQP Optimization.

As the previous case, it is possible to distinguish the vortices coming from the Suction Side and the ones coming from the periodic Pressure Side, as reported in Figure 59:

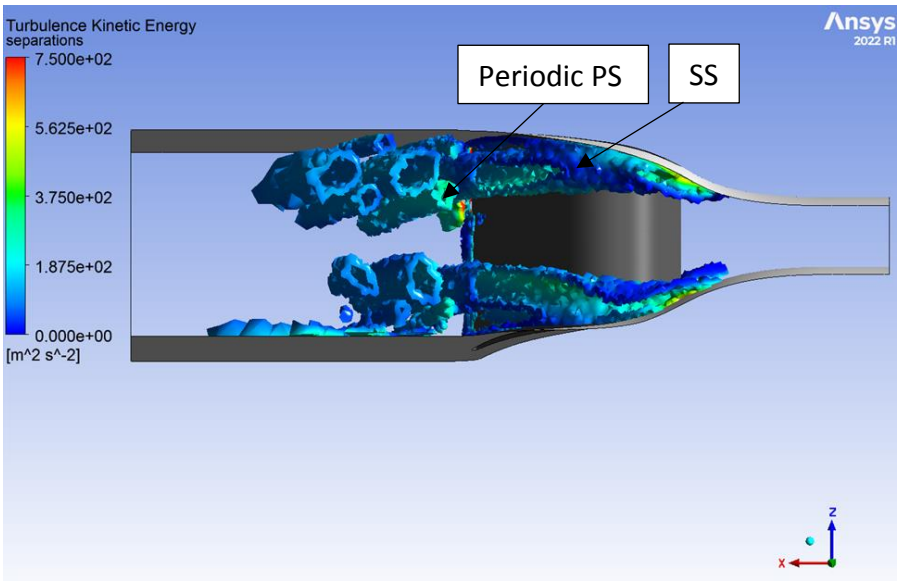

Figure 59: Lambda-2 Method for MISQP Optimization.

NLPQL Optimization Method Results

As already mentioned, the following configuration results to be equal to the one obtained with the previous method (MISQP) and therefore the results will not be analyzed in detail as for the other configurations.

The small decrease in the Efficiency reported in Table 9 is probably due to numerical approximations, therefore it is not possible to appreciate any difference with Mach Number and Total Pressure Contours of the previous case (Figure 56 and Figure 57).

In Figure 60 and Figure 61 are reported the Mach Number and Total Pressure contour for the NLPQL Optimization Method:

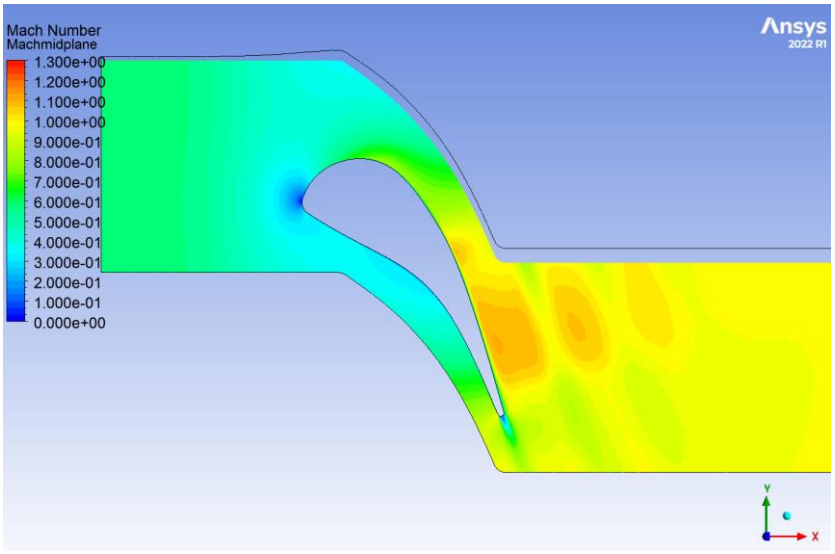

Figure 60: Mach Number Contour for NLPQL Optimization.

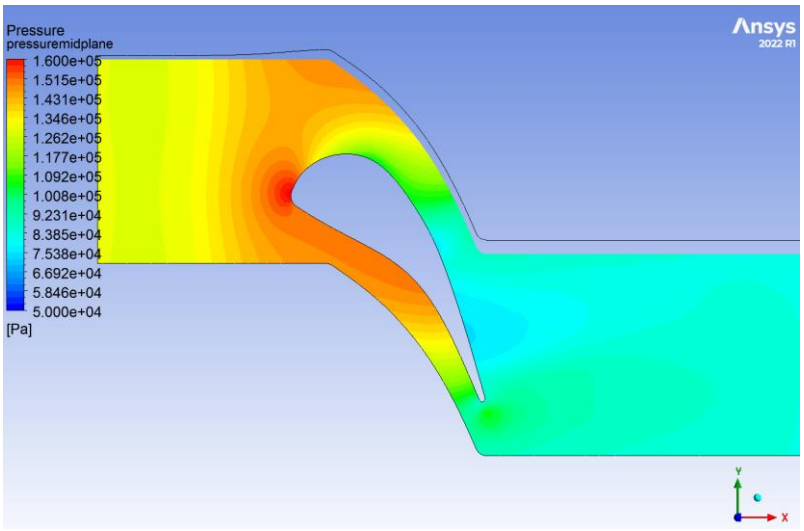

Figure 61: Total Pressure Contour for NLPQL Optimization.

MOGA Optimization Method Results

The last optimization method that is analyzed is the MOGA (Multiple Objective Genetic Algorithm) that can be used with more than one objective functions. For this analysis, the choice is to set the algorithm to reach the maximum possible efficiency, seeking zero angle coefficient. During the setup of the method it is possible to impose which objective function has more importance: in this case the Efficiency has more importance in respect of the Angle Coefficient, since the coupling of the vane with the rotor will be considered at another time.

Since this profile is the only one that has been optimized with a target that got to do with the Angle Coefficient, it is clearly visible that its shape is thinner in respect all the other optimized profiles. Therefore the outlet flow angle will be closer to the metal angle, but the Efficiency will be slightly lower, due to the shape of the vane.

In Figure 62 and Figure 63 are reported the Mach Number and Total Pressure contours: the first shock is smaller in respect of the previous cases while the second is the furthest to the boundary layer.

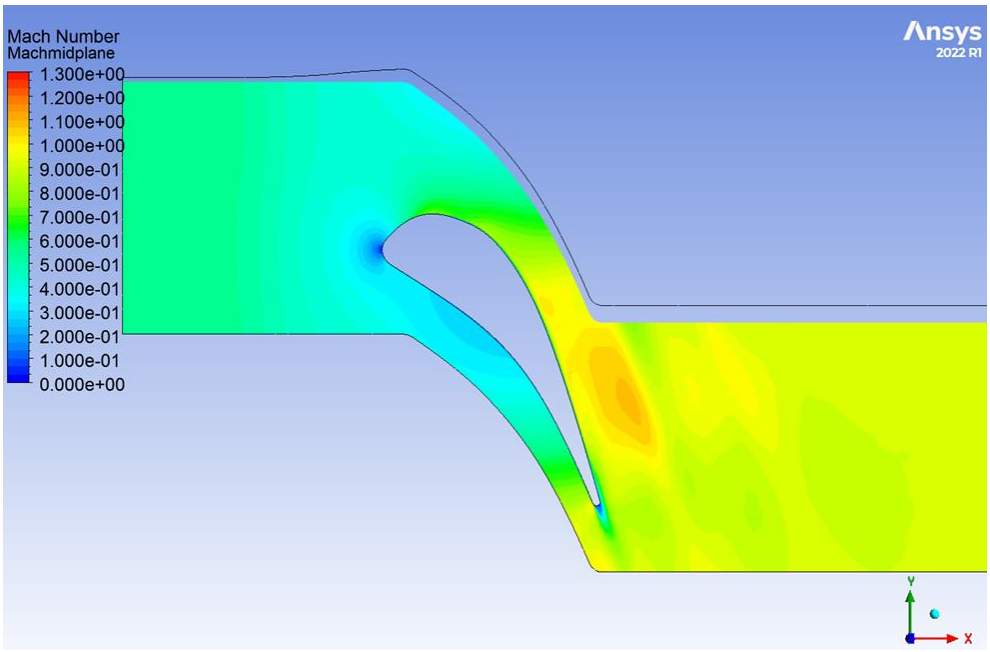

Figure 62: Mach Number Contour for MOGA Optimization.

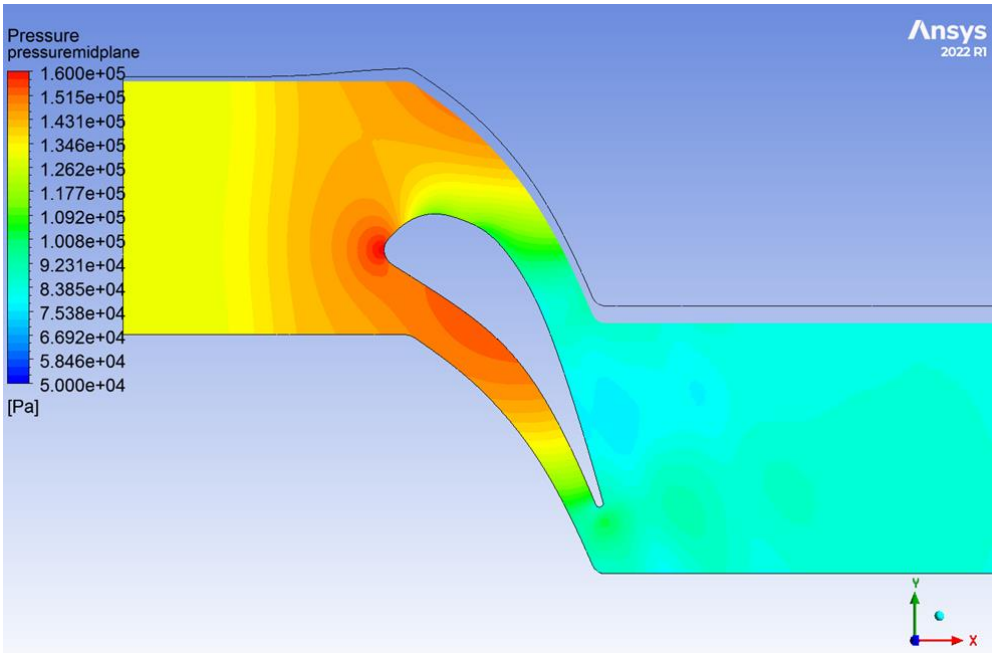

Figure 63: Total Pressure Contour for MOGA Optimization.

For this last configuration, the Lambda-2 Method shows a high increment in the vorticities and in the Turbulence Kinetic Energy intensity. In Figure 64 it is visible that the dissipated energy increased, therefore the following method has the lowest efficiency between the methods analyzed.

It is now possible to distinguish between the Diffusion Vortices due to the diffuser and the Horseshoe Vortices on the on Suction and Pressure Side:

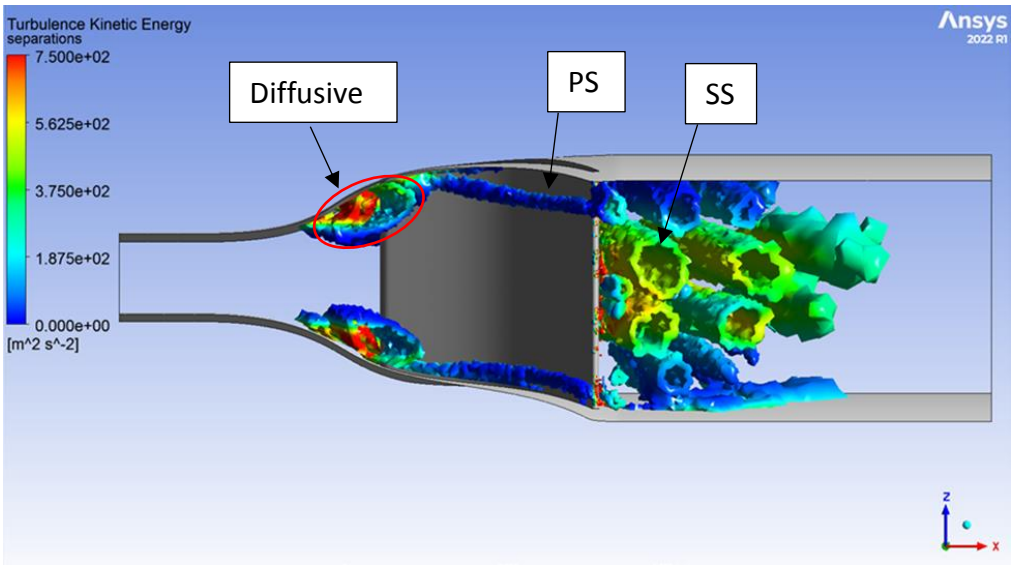

Figure 64: Lambda-2 Method for MOGA Optimization.

From Figure 65 it is visible how the vortices are generating in the diverging part of diffuser and are propagating towards the outlet of the vane moving closer to the midspan. This behavior is typical of blades showing Horseshoe vortices [31].

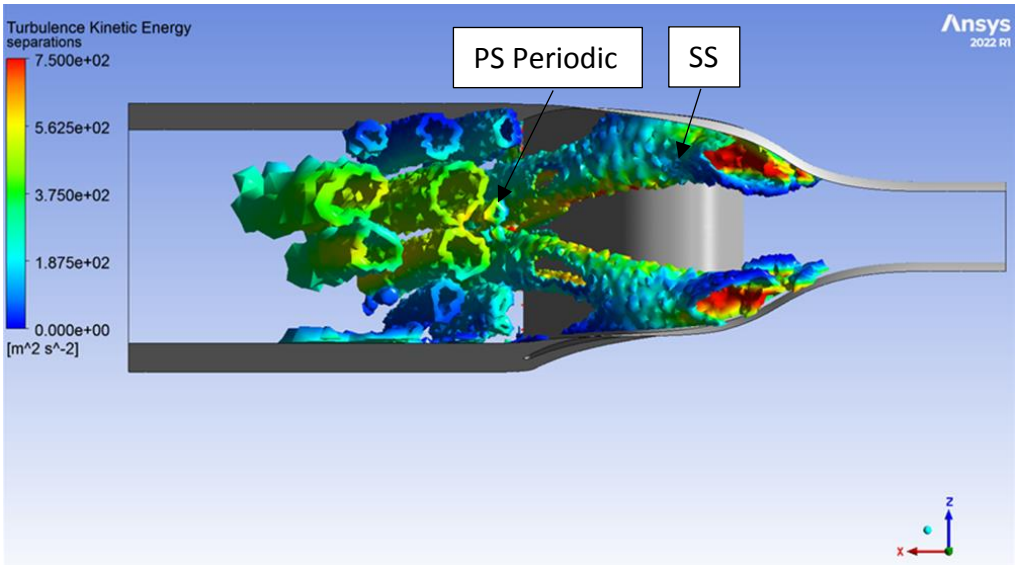

Figure 65: Lambda-2 Method for MOGA Optimization.

Blade Load Comparison

To conclude the comparison between the configurations obtained with different optimization methods it is reported the blade load of every case in respect of the CT3 Nominal Baseline.

In Figure 66 it is reported in Blue the Isentropic Mach Number distribution for the CT3 Nominal Vane: again it is visible how the MISQP and NLPQL Optimization Methods, whose Load is colored in yellow and purple, are overlapped, showing exactly the same behavior.

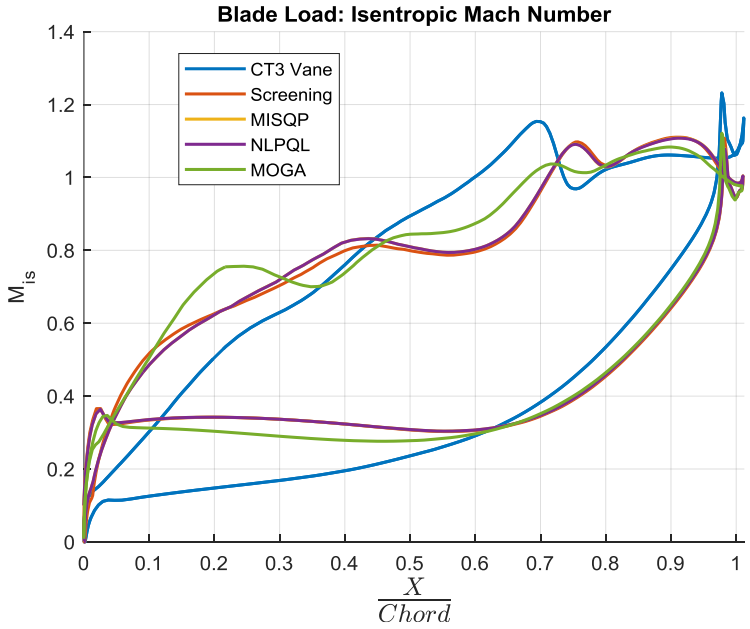

Figure 66: Vane Load: Isentropic Mach Number Comparison.

The CT3 Nominal Vane Load shows the highest spike at 70% of the chord, where the shock wave occurs and separations may be observed. In order to reduce as much as possible the separations on the Suction Side, it is suggested to move the chocking point as much as possible to the trailing edge, in order to move the separations occurring after the shock to the outlet of the vane. The Screening, MISQP and NLPQL methods are showing a smooth acceleration in the first part of Suction Side and a lower oscillation in respect the Nominal Vane at the highest spike at around 75% of the chord.

In Figure 67 the Static Pressure over Total Inlet Pressure Blade Load for every Optimized Vane is reported:

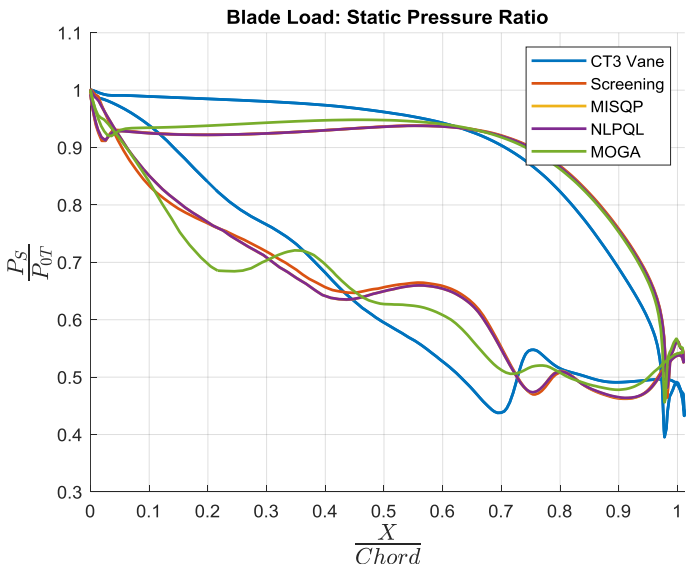

Figure 67: Vane Load: Static Pressure over Inlet Total Pressure Comparison.

Best Configuration Results: MISQP Optimization

From the considerations done during the analysis of the various optimized configurations, it is possible to state that the best solution found from the optimization is the one obtained with the MISQP method (Mixed-Integer Sequential Quadratic Programming).

First of all the contours of Mach Number and Pressure are reported for 25% span (Figure 68), 50% span (midspan, Figure 69) and 75% span (Figure 70): it is visible how the shape of the chocking area changes with the radial distance from the machine axis. At 25% span the chocking area is wider and has a higher Mach Number in respect than at mid-span and 75% span.

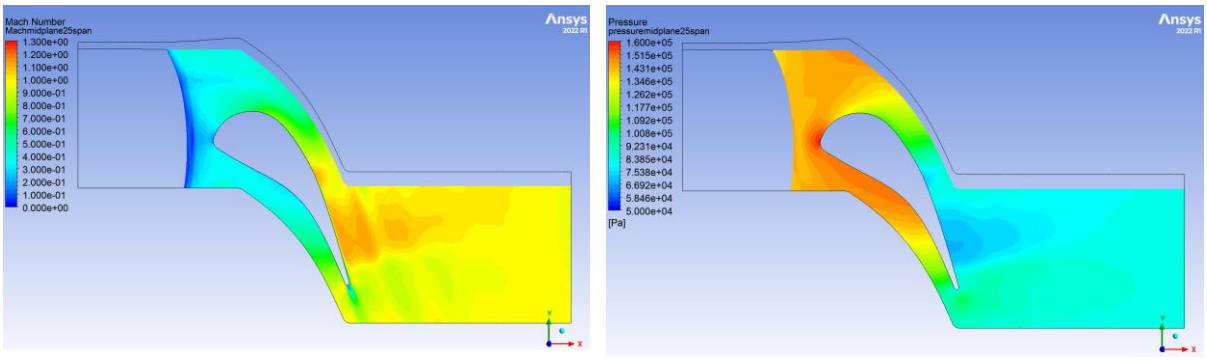

Figure 68: Mach Number and Total Pressure Contours at 25% span.

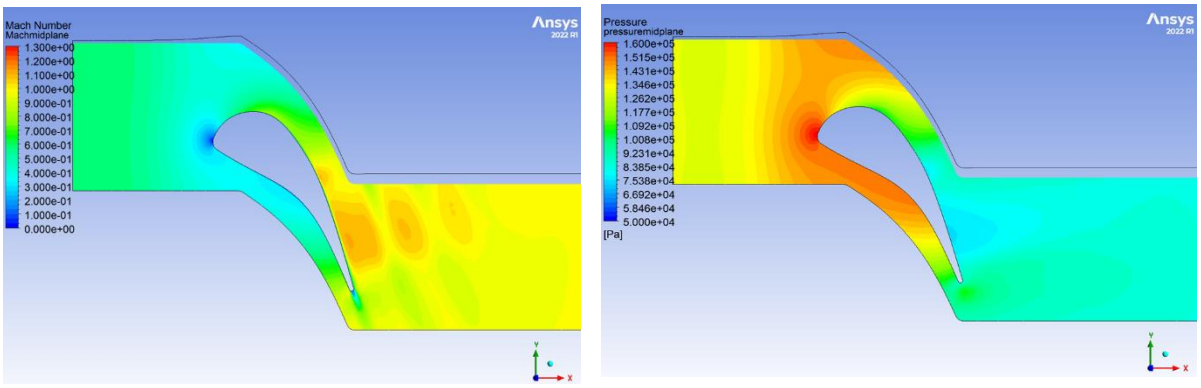

Figure 69: Mach Number and Total Pressure Contours at midspan.23

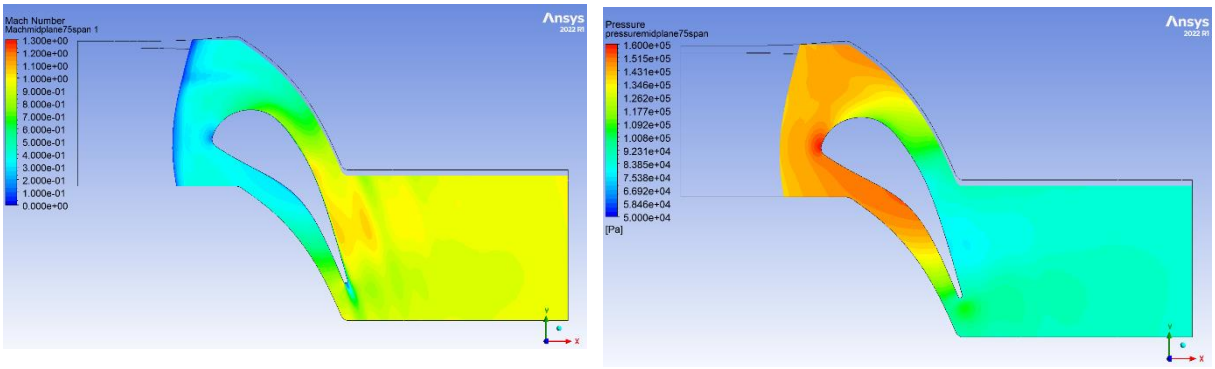

Figure 70: Mach Number and Total Pressure Contours at 75% span.

In Figure 71 are showed at mid-span the velocity vectors along the vane: No recirculation zones can be detected in this section and the flow seems to follow in the right way the vane profile.

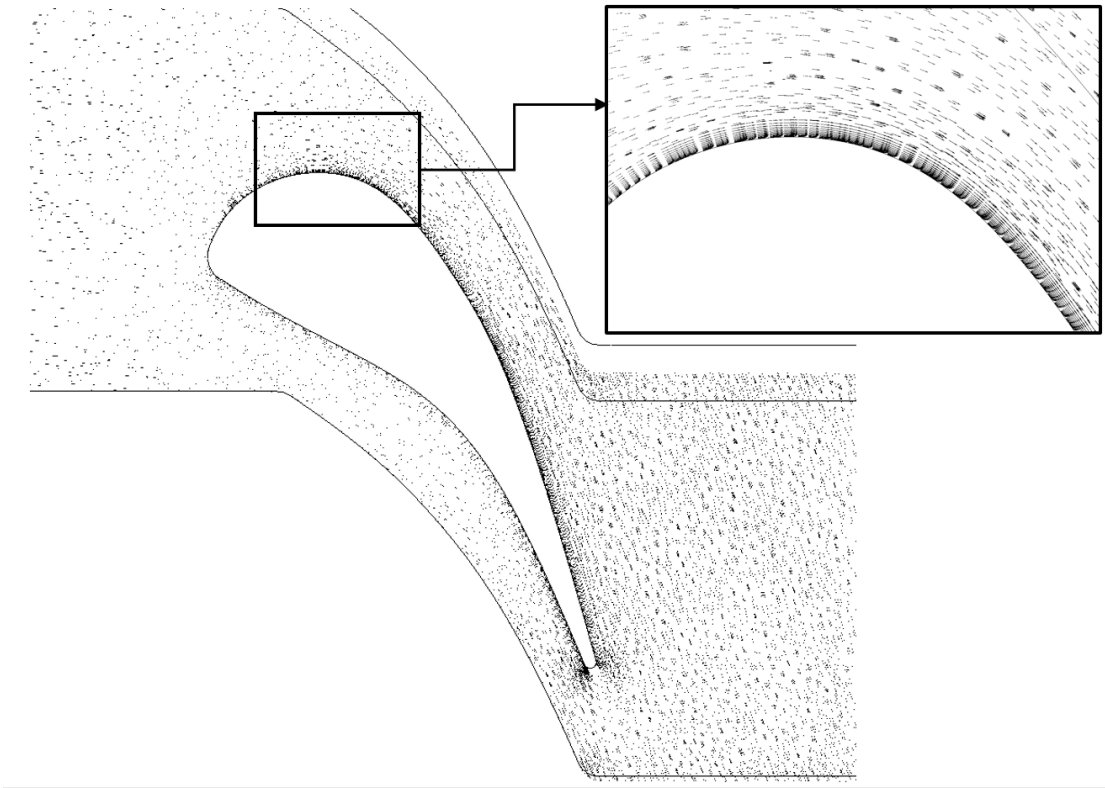

Figure 71: Velocity Vectors distribution along the blade on the X-Y midspan plane

In the meridional plane, instead, where the diffusive effects of the endwalls can be seen, some recirculation zones are detected: to better understand how the recirculating zones are distributed, four equidistant sections are defined in the Stator Domain, as can be seen from the following Figure 72 from Plane 1 to Plane 4:

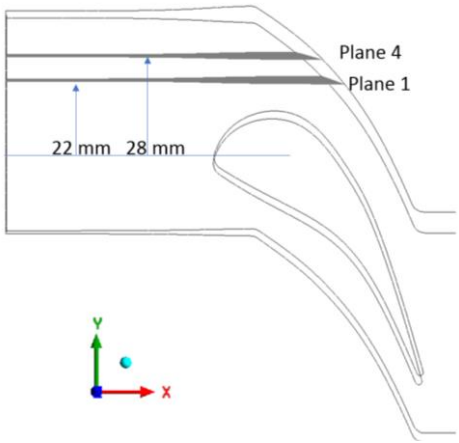

Figure 72: sketch of Stator on X-Y plane, with 2 of 4 planes considered.

For Every section on the X-Z plane, in Figure 73 are reported the details of Velocity Vectors Distributions: it is visible how the effect of the diffuser acts on the recirculation zones, that are increasing in width with the increase of Y distance in respect of the LE.

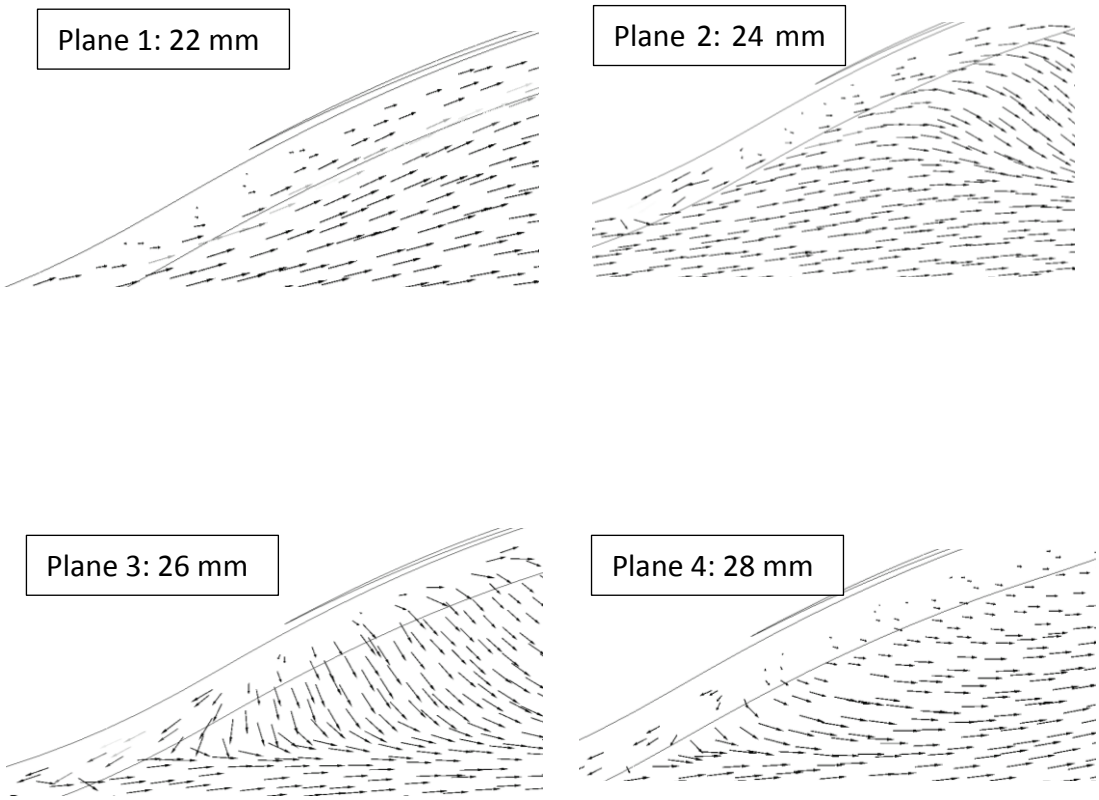

Figure 73: Details of the portion in Figure 74: Velocity Vectors Distribution on different X-Z planes.24

The Figure 73 shows a detail of the following portion, highlighted in red in the following Figure 74:

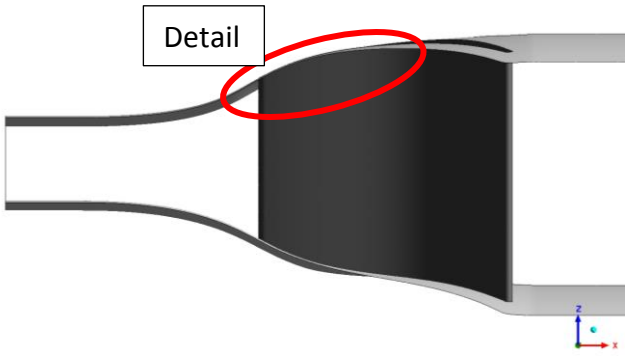

Figure 74: Portion considered in Figure 73 is highlighted in Red.

From Figure 73 it is possible to see that on Plane 1 a very small recirculation zone is present, while starting from the 2nd Plane, some zones of high inversion of flow can be detected especially at the beginning of the diffusive part, where it is clearly visible the

presence of inverse flow. There the particles are moving backwards, generating turbulences and vorticities as already mentioned during the Lambda-2 analysis.

At Plane 4, at 28 mm far from LE point on Y-axis, the dimension and intensity of recirculation is slightly reduced but still present. The presence of these recirculation zone leads to a decrease in the Efficiency of the vane, due to the dissipation of Energy.

Physical Parameters Comparison

As last step, a comparison between the Physical Parameters (already mentioned in the Chapter 3) of the Best Optimized Configuration (MISQP) and the Baseline configuration (CT3) is performed. To extract the Physical Parameters from the optimized profile, the same method mentioned in Chapter 3 is performed on the new geometry. As first step it is found the mean camber line in order to evaluate the maximum thickness, as shown in Figure 75:

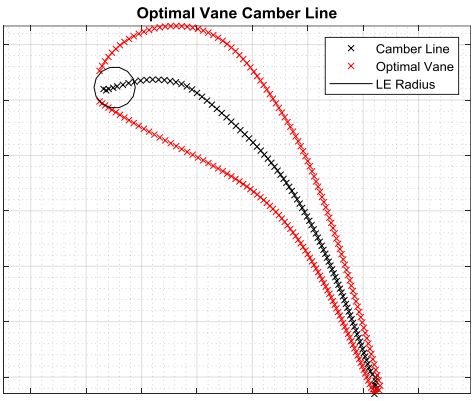

Figure 75: Camber Line obtained on Optimal profile.25

In Table 10 it is presented the comparison between the obtained values for MISQP Optimized Vane and CT3 Nominal one: it is visible how the Chord length is increased of around 6 mm in respect of the Nominal one. In Table all the dimension are normalized in respect of the Nominal Condition.

Table 10: Physical Parameters Comparison between Optimal and Nominal Profiles.

	CT3 Profile	GA-MISQP Profile
Chord [/]	1	1.089985486
Tmax [/]	1	1.052272727
LER [/]	1	0.974545455
TER [/]	1	0.83880597
Metal Angle [/]	1	1

Also the Thickness increased: indeed the percentage value in respect of the chord increased of more than one unit, meaning an increase of 3 mm in thickness.

Both the percentage values of LER and TER are decreased according to the increase in thickness, since the Leading and Trailing Edge depend on the maximum thickness value.

The metal angle is kept the same, since the points on the Trailing Edge are not changed during the Design of Experiments and the Optimal Stagger Angle is equal to zero.

In conclusion, the mean Camber Line obtained from this profile shows some differences with the Camber Line obtained with the nominal profile, analyzed in the Chapter 3 in Figure 1020: the Camber Line's gradient in correspondence of the change in slope on the Suction Side is higher for the Nominal CT3 Vane. In the Optimal Configuration, instead, the change in slope is smoother and takes place in a longer interval in respect the nominal one.

Chapter 8

Conclusions and Future Work:

During this Thesis the redesign of an already existing High-Pressure Stator is analyzed to study its integration with a Pressure Gain Combustor. In particular, starting from the existing CT3 Stator, an optimization is performed in order to optimize in terms of Efficiency and Outlet Flow Angle: the vane and the endwall shape are defined from some B-Spline curves controlled from Control Points, that change their position according upper and lower bounds. The endwall shape is changed from a configuration with constant span to a configuration with a diffusive shape, in order to control the area ratio of the stage, to change the Mach Number in Inlet, that has to be around 0.6.

Therefore the optimization is performed in order to satisfy the following requirements: Mach Number as close as possible to 0.6 (more than 3 times in respect the nominal value), Efficiency as high as possible and an Outflow Angle as much similar to the Metal Angle.

In order to run the Stator Optimization, a Design of Experiment is created starting from a Latin Hypercube Method to generate a set of 312 samples of 18 input parameters. 13 parameters are used to control some Control Points that define various vane geometries, 4 parameters are used to change the slope of the diffusive part of the endwalls and one to change the angle of stagger of the Vane.

With the generated DOE, a Response Surface is generated thanks to the Genetic Aggregation Response Surface Method and later optimized with all four possible Optimization methods proposed by ANSYS: Screening, Mixed-Integer Sequential Quadratic Programming (MISQP), Non-Linear Programming by Quadratic Lagrangian (NLPQL), and Multiple Objectives Genetic Algorithm (MOGA).

The best solution is obtained with the Mixed-Integer Sequential Quadratic Programming (MISQP) method and shows a Stator Efficiency equal to 95.57% with an Inlet Mach Number of 0.574 (close to the expected value of 0.6), a comparable mass flow rate in respect the baseline configuration and a low value of Angle Coefficient (equal to -0.0217).

It is necessary to perform further analysis over the coupling of this optimized configuration of the Stator with a Rotor, in order to explore the capability of subtracting work with the new Inlet Guided Vane (IGV) in respect to the Nominal Configuration of the CT3 Stage. To analyze the right integration with the new combustion model it is necessary that the next step of the study takes into account some un-steady boundary conditions typical of PGC, since for these preliminary analysis only steady state boundary

conditions have been considered. To correctly integrate the Turbine Stage with the PGC it is therefore necessary to modify the boundary conditions by adding fluctuations in the inlet pressure and temperature.

In this Study the Vanes and Walls have been considered without cooling flow and without any Heat Exchange with the Fluid. For this reason a further work will be also the analysis of the cooling system and Temperature Exchange, in order to reach more realistic results for what concerns the Pressure Gain Combustor and High-Pressure Turbine Coupling.

Bibliography:

[1] G. Paniagua Z. Liu J. Braun. Integration of a transonic high-pressure turbine with a rotating detonation combustor and a diffuser. Int J Turbo Jet Eng, 2020. doi: 10.1515/tjeng-2020-0016.

[2] G. Paniagua C. Xisto O. Petit T. Grönstedt A. Rolt A. Lundbladh. The efficiency of a pulsed detonation combustor–axial turbine integration. Aerospace Science and Technology, 2018. doi: 10.1016/j.ast.2018. 08.038.

[3] J. Sousa G. Paniagua E. C. Morata. “Thermodynamic analysis of a gas turbine engine with a rotating detonation combustor”. In: (2017). doi: 10.1016/j.apenergy.2017.03.045.

[4] https://aerospaceamerica.aiaa.org/year-in-review/taking-off-from-earth-to-space-with-pressure-gain-combustion-research/

[5] T. K. Jindal. “Pulse Detonation Engine – A Next Gen Propulsion”. In: (2012).

[6] R. Roda. “Pressure Gain Combustion”. In: (2015).

[7] New Argonne computational model to accelerate engine development for next-generation hypersonic flight By Jo Napolitano

[8] D. Schwer and K. Kailasanath. “Numerical investigation of rotating detonation Engine

[9] "Design and Analysis of Revolutionary Elevated Supersonic Axial Turbines", Nadupuru B. Rao, Rajesh CVS, Uppada Komali

[10] "Comprehensive Thermodynamic Analysis of the Humphrey Cycle for Gas Turbines with Pressure Gain Combustion", Panagiotis Stathopoulos.

[11] “Pressure-Gain Combustion for Gas Turbines Based on Shock-Flame Interaction”, . Eugen Lutoschkin. In: (2013).

[12] N. Billiard G. Paniagua R. Dénos. “Impact of Clocking on the Aero-Thermodynamics of a Second Stator tested in a One and a Half Stage HP Turbine.”. (2007).

[13] “Optimization of a Transonic High-Pressure Stage aimed at Coupling with Pressure Gain Combustors”, F. Civerra, D. Misul, N. Rosafio.

[14] https://en.wikipedia.org/wiki/Degree_of_reaction

[15] “Investigation of the Steady and Unsteady Performance of a Transonic HP Turbine”, G. Paniagua.

[16] J. Dunham, “A Parametric Method of Turbine Blade Profile Design”, National Gas Turbine Estabilishment, Peyestock, Farnborough.

[17] "Computer Program to Obtain Ordinates for NACA Aerofoils." Ladson, Brooks, Hill & Sproles, NACA Langley, NASA TM-4741.

[18] “Aero-Thermal Performance of a Two Dimensional Highly Loaded Transonic Turbine Nozzle Guide Vane: A Test Case for Inviscid and Viscous Flow Computations”, Von Karman Institute, M. Lambert.

[19] https://www.hpc.polito.it/index.php

[20] https://cran.r-project.org/web/packages/lhs/vignettes/lhs_basics.html#X

[21] wb. https://forum.ansys.com/forums/topic/genetic-aggregation-is-default-response-surface/

[22] https://ansyshelp.ansys.com/account/secured?returnurl=/Views/Secured/corp/v221/en/wb_dx/dxUsingMetaModelTypes.html

[23] https://ansyshelp.ansys.com/account/secured?returnurl=/Views/Secured/corp/v221/en/wb_dx/dxTheoGeneticAgg.html?q=moving%20least%20square

[24] https://en.wikipedia.org/wiki/Moving_least_squares

[25] “One-Step Screening and Process Optimization Experiments”,John Lawson

[26] “The multi-objective genetic algorithm optimization, of a superplastic forming process, using ansys”, G. Grebenisan, N. Salem.

[27] https://ansyshelp.ansys.com/account/secured?returnurl=/Views/Secured/corp/v221/en/wb_dx/dxBEMtemp13.html?q=NLPQL

[28] https://ansyshelp.ansys.com/account/secured?returnurl=/Views/Secured/corp/v221/en/wb_dx/dx_theory_MISQP.html

[29] “Unsteady Methods Applied to a Transonic Aeronautical Gas Turbine Stage” Giorgio Amatoa*, Matteo Giovanninia, Michele Marconcini, Andrea Arnone.

[30] J. Jeong and F. Hussain. On the Identification of a Vortex. J. Fluid Mechanics, 285:69-94, 1995.

[31] “Secondary Flow Measurements in a Turbine Passage With Endwall Flow Modification”, N. Aunapu, K. Flack, R. Stoddard, R. Volino.

Acknowledgements

I would like to express my deepest appreciation to Professor Simone Salvadori for the support and the attentions provided during this activity. Thanks to your constructive advices and practical suggestions the development of the project was carried out with pleasure.

I would also like to extend my deepest gratitude to Professor Daniela Anna Misul for her professional and personal support. With your kindness and interest, you inspired me to follow the research activity in this field of study.

I'm extremely grateful to my three supervisors, the PhD Students Rosario Nastasi, Gallis Panagiotis and Nicola Rosafio, whose patience cannot be underestimated. I want to express my thanks to you, for your unwavering support and ingenious suggestions during my activity.